Proceedings of the Combustion Institute 42 (2026) 106299

Contents lists available at ScienceDirect

Proceedings of the Combustion Institute

journal homepage: www.elsevier.com/locate/proci

Dynamics of flame initiation, propagation, and transition to detonation

Zheng Chen [a,*], Wang Han [b], Tianhan Zhang [b]

[a] SKLTCS, HEDPS, School of Mechanics and Engineering Science, Peking University, Beijing 100871, China
[b] School of Astronautics, Beihang University, Beijing 100191, China

ARTICLE INFO

Keywords:
Premixed flames
Forced ignition
Autoignition
Flame propagation
Detonation

ABSTRACT

Understanding of flame initiation, propagation, and transition to detonation is vital for both fundamental combustion science and practical applications, including the development of high-performance engines and the enhancement of explosion safety. This paper reviews recent progress in the flame dynamics and critical physical conditions governing these interconnected processes, focusing on *laminar, premixed, gaseous* mixtures. First, recent advances in forced ignition of premixed flames are reviewed, with an emphasis on theoretical analysis of critical ignition radius and minimum ignition energy. The effects of low-temperature chemistry and imposed flow on forced ignition of premixed flames are also discussed. Subsequently, flame propagation into autoigniting mixtures is addressed. Under engine-relevant high-temperature and high-pressure conditions, the ignition delay of the end-gas can become comparable to the flame transit time, leading to end-gas autoignition, autoignition-assisted flames, and cool flame development and transition to hot flame. Finally, the dynamics of autoignition-induced transition to detonation are analyzed, with a focus on the mechanism for detonation development in autoigniting mixtures. Throughout the paper, the continuous physical chain—from ignition kernel initiation to flame propagation and ultimately to detonation transition—is emphasized.

Novelty and significance statement: This review uniquely connects forced ignition, flame propagation into autoigniting mixtures, and transition to detonation. It presents recent theoretical advances in premixed flame ignition, end-gas autoignition, and detonation development. The role of low-temperature chemistry in reducing ignition energy, enabling flame propagation, and promoting detonation development is highlighted. The paper also discusses flow-facilitated ignition, autoignition-assisted flame speed scaling, and practical implications for detonation development in engines, thereby offering a systematic foundation for controlling extreme combustion events.

1. Introduction

The interaction between chemical reactions and fluid dynamics gives rise to a rich spectrum of combustion phenomena. Among these, the unsteady processes of flame initiation, its subsequent propagation, and the potential for a sudden transition to detonation represent a cornerstone of combustion physics. These three processes — encapsulated in the dynamics of deflagration-to-detonation transition (DDT) [1–9] — are not merely an academic curiosity but a critical consideration across a vast array of practical applications.

In the energy sector, uncontrolled DDT poses a paramount safety concern in the design of hydrogen fuel systems [10], nuclear reactor containment [11–13], and the transport and storage of hydrocarbon fuels [14,15]. Conversely, the same phenomenon is the fundamental operational principle behind pulsed, rotating and oblique detonation engines (PDEs, RDEs and ODEs), which are promising for next-generation propulsion and power generation [16–26]. Therefore, a profound understanding of the mechanisms governing ignition, flame propagation and acceleration, and final leap to detonation is essential for both mitigating industrial hazards and harnessing the power of the most extreme form of controlled reactive flow.

The journey from a quiescent, reactive mixture to a fully developed detonation is a complex process that begins with the creation of a flame kernel. This introductory section presents the fundamental aspects and backgrounds of forced ignition of premixed flames, flame propagation and its interaction with autoignition under engine-relevant conditions, and the transition to detonation and DDT.

Flame initiation. *Forced ignition* is the primary means of initiating combustion in practical devices such as internal combustion engines (ICEs) and gas turbines [27–34]. It can be achieved by an electrical spark, a laser pulse, or a hot surface. Under conventional conditions ignition is straightforward, but modern trends toward ultra-lean mixtures, low-pressure (e.g., high-altitude relight) or high-speed (e.g., scramjet) environments make it increasingly difficult [35–37].

* Corresponding author.
E-mail address: cz@pku.edu.cn (Z. Chen).

https://doi.org/10.1016/j.proci.2026.106299
Received 15 April 2026; Accepted 9 June 2026

In a quiescent mixture, forced ignition proceeds through three stages: hot-kernel formation, reaction-front expansion, and transition to a self-sustained flame [38,39]. The early kernel experiences large positive stretch due to its small radius. Consequently, the minimum ignition energy (MIE) and critical radius strongly depend on the Lewis number: positive stretch promotes ignition for $Le < 1$ and inhibits it for $Le > 1$ [40–43]. The MIE increases quickly with Lewis number and thereby it is challenging to ignite mixture with large Le [34].

In addition, real fuels exhibit multi-stage autoignition due to low-temperature chemistry (LTC). For instance, n-heptane shows a negative temperature coefficient (NTC) regime and can form cool and warm flames before hot ignition [44,45]. LTC and cool flame might affect MIE and alter flame dynamics. While cool flames have recently received considerable interest, the bulk of existing research has concentrated on flame speed and extinction boundaries [44,45]. In contrast, the forced ignition of cool flames remains comparatively underexplored, warranting further systematic study.

Besides chemistry, the flow environment also profoundly affects forced ignition. Flow and turbulence induce stretch and convective heat loss and thereby affect ignition kernel development. Counter-intuitively, turbulence may sometimes facilitate ignition [33,46,47], but the underlying mechanisms are still contradictory between experiments [46,47] and numerics [48]. How flame stretch, differential diffusion, heat loss to electrodes, and turbulent dissipation collectively affect ignition remains unclear, requiring further combined experimental and numerical studies.

Flame propagation. Once a flame kernel becomes self-sustained, *flame propagation* ensues. Premixed flames are typically assumed to propagate into frozen mixtures without upstream reactions [49–55]. In practice, however, the unburned gas is often pre-compressed. Under engine-relevant high-temperature and high-pressure conditions, the ignition delay of end-gas can become comparable to the flame residence time [56–58]. Autoignition may then occur ahead of the flame, yielding combustion mode transition from normal flame propagation to end-gas autoignition or even detonation [57,58].

Engine knock is generally accepted to result from end-gas autoignition [56–58], occurring when the local ignition delay falls below the time for the flame to consume the end-gas. Strong mutual enhancement between flame propagation and autoignition can occur in engines [57], underscoring the need to understand their interaction.

For fuels exhibiting NTC behavior, multi-stage ignition adds more complexity [45]. A cool flame, raising temperature by only 200–300 K, can propagate as a self-sustaining front and sensitize the mixture for subsequent hot ignition, introducing flame-autoignition interaction. Consequently, the presence of cool/warm flames, along with differential diffusion and flame stretch (characterized by Lewis and Markstein numbers), introduces additional complexity to the dynamics of flame propagation into autoigniting mixtures.

In addition, spherical flame propagation after central ignition in an initially static mixture is popularly used to measure the laminar flame speed S_u [59–63]. Usually S_u is measured in chemically frozen mixtures. Recently, expanding spherical flames in constant-volume spherical chambers [64–69], shock tubes [70–77], and rapid compression machines (RCMs) [78–81] have been used to obtain S_u under high-temperature and high-pressure environments where the flame interacts with pre-ignition chemistry. Therefore, flame-autoignition interaction and autoignition-assisted flames are current hot topics in fundamental flame dynamics.

Transition to detonation. The third key process is the *transition from premixed flame propagation to detonation*. Under strong acceleration, a flame generates compression waves that coalesce into a leading shock. This shock compresses the unburned gas and thereby accelerates flame propagation. When the reaction front couples coherently with the shock, a supersonic detonation wave forms, characterized by a leading shock followed immediately by a reaction zone [5]. The exact mechanism of DDT has been debated for decades and remains a major challenge in combustion science [1–9].

Similar to flame propagation, detonation development and DDT have been mainly considered for chemically frozen mixtures [1–9]. Unlike previous studies [1–9], this paper focuses on transition to detonation in an autoigniting mixture. Under engine-relevant conditions, the end-gas may autoignite ahead of the flame. This volumetric autoignition can generate pressure waves that, under suitable conditions, couple with the reaction front and evolve into a detonation.

For detonation development in autoigniting mixtures, Zel'dovich's reactivity gradient theory [82,83] provides a fundamental framework. Bradley and co-workers [84,85] subsequently introduced the "detonation peninsula" to determine critical conditions for detonation development. However, the boundaries for detonation development depend on many factors, including thermal conditions (temperature and pressure), mixture composition (equivalence ratio and dilution), fuel type, and temperature distribution in a hot spot. Recent studies have tried to elucidate the influence of these factors on the detonation regime and underlying mechanisms. A major challenge remains in applying these boundaries to predict detonation development in practical engines with complex turbulent flows and real multi-component fuels.

In spark-ignition engines (SIEs), detonation development in autoigniting mixtures is responsible for super-knock and should be prevented [57,58]. Similar DDT-like phenomena have also been observed/hypothesized in scramjet engines [86,87], and autoignition might assist detonation initiation in rotating and oblique detonation engines [17–24]. Therefore, this review focuses on the less-explored but practically important regime of detonation development in autoigniting mixtures.

Scope and outline. This paper reviews recent progress in the dynamics and critical physical conditions governing premixed flame ignition, propagation and transition to detonation. It mainly focuses on combustion in *laminar, premixed, gaseous* mixtures. Rather than suggesting a universal progression from ignition to detonation, this paper concentrates on selected links among ignition, flame propagation, and the transition to detonation. For flame propagation and DDT, this paper mainly focuses on autoigniting mixtures (for which the ignition delay time is comparable to the characteristic flame time) rather than chemically frozen mixtures. It is noted that numerous DDT scenarios involve only flame acceleration and gas-dynamic feedback, without end-gas autoignition. Besides, in many cases of forced ignition and flame propagation, especially in chemically frozen mixtures, the process never approaches DDT.

The remainder of this paper is organized as follows (see Fig. 1). Section 2 reviews recent advances in forced ignition of premixed flames, with emphasis on recent theory determining the critical ignition radius and minimum ignition energy. The effects of chemistry, flow and transport on forced ignition are also examined. Section 3 addresses flame propagation and its interaction with autoignition under high-temperature and high-pressure conditions. End-gas autoignition, flame-autoignition interaction, and cool flame propagation are discussed. Section 4 analyzes the final stage – the transition to sustained detonation. The mechanisms by which compression waves coalesce into a leading shock, and the conditions under which the reaction front couples with the shock to form a self-sustained detonation wave, are discussed. The recent progress in understanding detonation development in engines is also presented. Finally, concluding remarks and suggestions for future research are presented in Section 5.

2. Forced ignition of premixed flames

Ignition is the process by which a flammable medium is brought to a rapid combustion state [27]. There are two types of ignition: autoignition and forced-ignition. Autoignition, also called self-ignition, is caused by chain branching or thermal feedback in a homogeneous mixture without input of either an external source of thermal energy

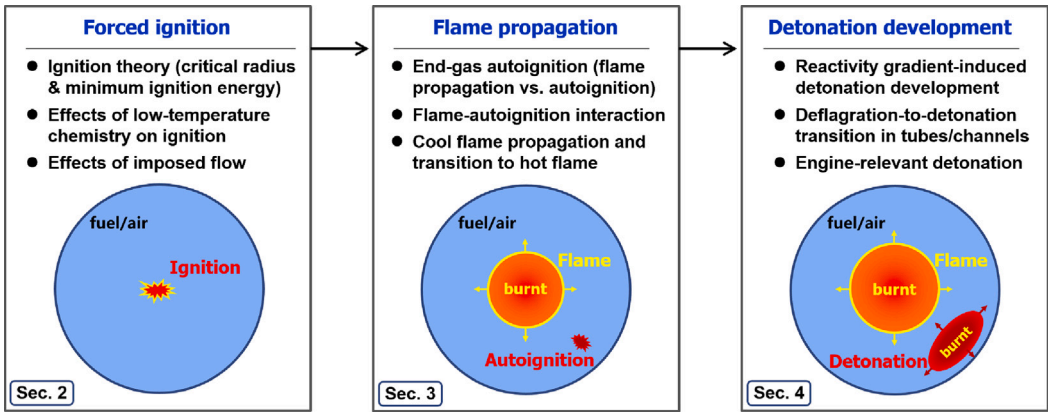

Fig. 1. Schematic of contents covered in Sections 2, 3 and 4.

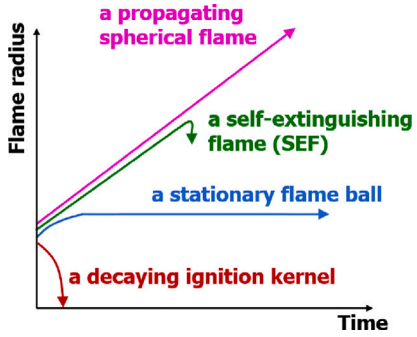

Fig. 2. Different outcomes of forced ignition in a quiescent mixture.

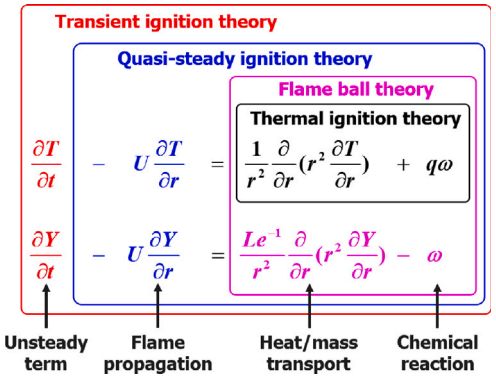

Fig. 3. Different ignition theories considering various terms in the non-dimensional equations for temperature and mass fraction of the deficient reactant. Reprinted from [34].

or active radicals into the system. Unlike autoignition, forced-ignition is the result of electrical discharge (spark), heated surface, shock wave, or pilot flame, with the locally initiated flame front subsequently evolving into a self-propagating state where the ignition source can be removed without extinguishing the combustion process. This section focuses on forced-ignition in a gaseous mixture. First, recent progress in premixed flame ignition theory is introduced. Then, the effects of low-temperature chemistry and imposed flow on the forced ignition process are discussed.

2.1. *Premixed flame ignition theory*

Forced ignition of a quiescent premixture is a fundamental combustion process. Depending on mixture composition, thermal state, and energy deposition, different outcomes can occur (Fig. 2). If the ignition energy is insufficient or the mixture lies outside its flammability limits, the ignition kernel decays, and ignition fails. In contrast, with sufficient energy and a mixture within the flammability limits, the ignition kernel grows into a self-sustained spherical flame, indicating a successful ignition. For mixtures near or below the flammability limit with a low Lewis number, self-extinguishing flames or stationary flame balls can form under microgravity conditions [88,89].

Over the past century, theoretical studies on forced ignition have progressively incorporated more realistic physics, evolving from simple thermal balance models to fully transient descriptions. Fig. 3 illustrates the physical and chemical processes incorporated in various ignition theories. The governing equations are written in a coordinate frame moving with the flame front at normalized speed U [42]; thus, the convection term accounts for flame propagation. Classical thermal ignition theory considers the balance between conductive heat loss and chemical heat generation. Flame ball theory further includes reactant transport alongside heat transport, as flame chemistry involves both heat release and fuel consumption. Quasi-steady ignition theory describes the transition from an ignition kernel to a self-sustained spherical flame. As highlighted by the blue box in Fig. 3, it includes the convection term (flame propagation) but neglects unsteady kernel evolution. Transition ignition theory additionally incorporates the unsteady term, making it the most comprehensive ignition theory to date. A comprehensive review on premixed flame ignition theory is provided by Yu and Chen [34]; and only key theoretical developments are summarized below.

Thermal ignition theory. The thermal ignition theory [90,91] determines the critical ignition conditions by balancing chemical heat release inside a spherical ignition kernel with conductive heat loss to the surroundings. The kernel is considered to be at the adiabatic flame temperature T_{ad}, while the unburned gas is at T_u. The critical kernel size is determined by the condition that the rate of heat generation inside the kernel equals the rate of heat conduction from its surface. This yields a minimum radius R_{cr} below which conductive loss dominates and the kernel extinguishes. The energy balance yields $R_{cr} \sim \delta_L = \alpha/S_L$, i.e., the minimum flame kernel is comparable to the laminar flame thickness [90,91] . The MIE is then $E_{\min} \sim \frac{4}{3}\pi(\delta_L)^3\rho_u c_p(T_{ad}-T_u)$.

The thermal ignition theory provides a clear physical picture and can successfully explain the effects of pressure, dilution, and equivalence ratio on ignition. For example, at low pressure or near flammability limit, the flame thickness δ_L^0 increases, leading to a large critical radius and thus a high $E_{\min}$, which explains why ignition becomes extremely difficult under such conditions. However, the theory neglects mass diffusion and reactant consumption; and thereby it cannot account for Lewis number effects. Moreover, it ignores flame stretch and kernel propagation, making it inaccurate for mixtures with $Le \neq 1$.

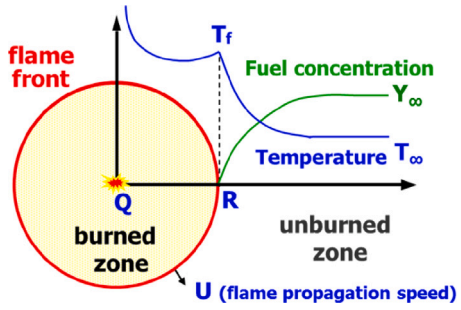

Fig. 4. Schematic flame structure for ignition and propagation of spherical flames. The flame propagation speed U and flame temperature T_f both change with the flame radius R.

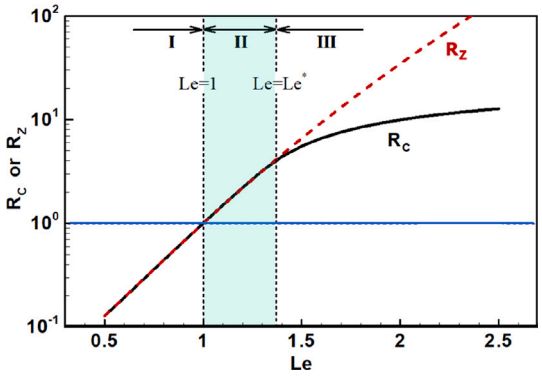

Fig. 5. Change of the critical flame radius and the flame ball radius with the Lewis number. Reprinted from [43].

Flame ball theory. The flame ball theory, pioneered by Zel'dovich [90], considers a stationary spherical flame in a quiescent combustible mixture, sustained solely by the diffusion of heat and mass without any imposed flow. The flame front is at rest, and the deficient reactant is supplied entirely by molecular diffusion from the surroundings. The characteristic equilibrium radius —— the flame ball radius, R_Z —— is found to depend strongly on the Lewis number $Le = \alpha/D$ (thermal diffusivity over mass diffusivity) [90]. Stability analysis showed that an adiabatic flame ball is inherently unstable: a small perturbation causes either inward collapse (extinction) or outward propagation (successful ignition). Therefore, the flame ball radius R_Z was considered as the critical length controlling premixed flame ignition [8,90] and the MIE was proposed to be proportional to the cube of the flame ball radius instead of the flame thickness, $E_{\min} \sim R_Z^3$. The theory shows that the flame ball radius R_Z and flame temperature T_f depend strongly on Le: for $Le < 1$ (e.g., lean H_2/air), R_Z is smaller than the laminar flame thickness and T_f exceeds the adiabatic flame temperature, promoting ignition; for $Le > 1$ (e.g., lean heavy hydrocarbons), the opposite occurs, making ignition more difficult.

The flame ball theory incorporates both heat and mass diffusion, thereby accounting for Lewis number effects. It explains why mixtures with $Le > 1$ are more difficult to ignite. However, this theory neglects flame kernel propagation and stretch. The critical ignition radius derived from flame ball theory overestimates the actual R_{cr} for mixtures with large Lewis number, and it cannot describe the dynamic evolution of an expanding flame kernel.

Quasi-steady ignition theory. The thermal theory and flame ball theory on premixed flame ignition do not consider the ignition kernel propagation. The ignition kernel has very large curvature and is highly stretched during its outward propagation. Therefore, the coupling between positive stretch rate and preferential diffusion between heat and mass (i.e., Lewis number) is expected to greatly affect the ignition kernel propagation and the critical ignition conditions. Considering this fact, the quasi-steady theory on ignition was developed [41,42]. The model is shown in Fig. 4, in which ignition is caused by heat flux at the center and the spherical flame propagates outwardly. The change of flame propagation speed U with the flame radius R depends on the ignition power at the center, Lewis number and radiative heat loss [42].

For adiabatic propagating spherical flames, the following equations for flame propagating speed U (normalized by adiabatic planar flame speed), flame radius R (normalized by adiabatic planar flame thickness), and flame temperature T_f (normalized by adiabatic flame temperature increase) is obtained [42]:

$$\frac{T_f R^{-2} e^{-UR}}{\int_R^\infty \tau^{-2} e^{-U\tau} d\tau} - QR^{-2}e^{-UR} = \frac{1}{Le}\frac{R^{-2}e^{-ULeR}}{R} = \exp\left[\frac{Z}{2}\frac{T_f - 1}{\sigma + (1-\sigma)T_f}\right] \quad (1)$$

where Le, Z, and σ are, respectively, the Lewis number, Zel'dovich number, and the ratio of burned to unburned gas densities. The ignition power, Q, is provided as a heat flux at the center (see Fig. 4). By solving Eq. (1) numerically, the relations for the flame propagating speed, flame radius, and flame temperature, as well as the existence of different flame regimes for different Lewis numbers and/or ignition powers can be obtained [42,43].

It is found that for each mixture at a given Lewis number, there is a critical flame radius, R_C, above which the flame can successfully propagate outward and eventually become a planar flame [42,43]. No quasi-steady solution exists below the critical flame radius. Therefore, to successfully initiate a spherical flame, the ignition source must be large enough to sustain a flame to a radius beyond R_C.

Fig. 5 shows the variation of the critical flame radius and the flame ball radius (both normalized by the flame thickness) with Lewis number. They are both shown to depend strongly on the Lewis number. Three regimes in terms of the Lewis number are observed [43]. In regimes I and II, with a Lewis number less than $Le^* = 1.36$, the critical flame radius is the same as the flame ball radius and it is smaller/larger than the flame thickness when the Lewis number is below unity (regime I)/above unity (regime II). In regime III, with $Le > Le^*$, the critical flame radius is smaller than the flame ball radius but larger than the flame thickness. The difference between the critical flame radius and the flame ball radius/flame thickness is of order-one magnitude when $Le > 2.0$. As a result, the MIE is substantially over-predicted/under-predicted based on the flame ball radius/flame thickness for mixtures with large Lewis numbers [43]. Therefore, the flame ball radius can be considered as the flame initiation controlling length only for mixtures with $Le < Le^*$ while the flame thickness only for $Le = 1$.

The quasi-steady ignition theory has the advantages that it incorporates flame stretch and preferential diffusion, correctly predicting the Lewis number effect and showing that the flame ball radius overestimates MIE for large Le. However, it assumes quasi-steady propagation, neglects unsteady terms, and cannot evaluate MIE for finite-duration heating.

Transient ignition theory. All the above theories assume either a constant heat source or an instantaneous deposition, and they neglect the unsteady term in the governing equations. The transient ignition theory developed by Yu and Chen [38] removes these limitations. It solves the time-dependent energy and species equations for a finite-duration heating source, using a coordinate transformation that maps the moving flame front to a fixed domain. The theory reveals a "memory effect" [38]: after the external heating is switched off, the flame kernel can continue to propagate for some time because of the thermal and chemical energy already deposited. This memory effect reduces the MIE compared to quasi-steady predictions, especially at high heating

Table 1
Different ignition theories considering various controlling physical/chemical processes.

Theory	Governing Physics/Chemistry	Limitations/Key findings
Thermal Ignition Theory	Balance between chemical heat release and conductive heat loss.	Neglects mass diffusion and reaction depletion of fuel. The critical ignition length scale is the flame thickness δ_L, and MIE $\sim \delta_L^3$.
Flame Ball Theory	Considers the balance between chemical heat release and conductive heat loss as well as the balance between mass diffusion and reaction depletion of the deficient reactant.	No flame propagation. The critical ignition length scale is the flame ball radius R_Z and MIE $\sim R_Z^3$, showing strong Lewis number (Le) dependence.
Quasi-Steady Ignition Theory	Considers flame kernel propagation (convection term) in a quasi-steady state manner, coupling heat/mass transport with flame stretch.	No temporal memory of energy deposition. Demonstrates that R_{cr} differs from both δ_L and R_Z, especially for $Le > 1$.
Transient Ignition Theory	Incorporates unsteady terms in governing equations and finite-duration energy deposition.	Most complete theory considering one-step global chemistry. Captures "memory effect" of heating.

powers. As the heating power increases, the MIE predicted by the transient theory asymptotically approaches a finite lower bound, whereas the quasi-steady MIE continues to increase without bound – an non-physically behavior. The transient theory also explains why repetitive heating pulses (e.g., nanosecond repetitively pulsed discharges) can reduce the MIE: each subsequent pulse revitalizes the kernel before it extinguishes [92,93].

Table 1 summarizes the various controlling physical and chemical processes considered in different ignition theories as well as their limitations.

In all the studies mentioned above, one-step, irreversible, global reaction models were employed, and thus the role of energetic active radicals was not considered. In practical combustion of hydrocarbon fuels, elementary reactions related to fuel and reactive intermediate species appear [94]. Zhang et al. [95,96] analyzed the spherical flame initiation and propagation with thermally sensitive intermediate kinetics [94] within the framework of large activation energy and quasi-steady assumptions. The minimum chemical and thermal ignition powers were compared and it was found that for most cases, heat deposition is more efficient in ignition than radical addition [95,96]. The above ignition theories were developed for gaseous mixtures, while fuel droplets might appear during the forced ignition in engines. Han and Chen [97] developed ignition theory for spherical spray flames with finite-rate droplet evaporation. It shows that droplet load and vaporization Damköhler number significantly affect flame propagation speed, Markstein length, and minimum ignition power. For lean mixtures, increased effective Lewis number makes ignition much more difficult than for rich mixtures.

The above ignition theories have the advantage of clearly revealing the physicochemical mechanisms that control ignition. However, an important limitation is their difficulty in incorporating complex reactions, such as LTC and cool flames which may affect the ignition process. This will be discussed in the following subsection. Moreover, practical ignition is often probabilistic, as electric spark breakdown is inherently stochastic [29,33]. Consequently, unlike the sharp deterministic threshold of MIE predicted by theory, experimental determination of MIE typically relies on statistical methods — such as logistic regression — to obtain the value corresponding to a 50% ignition probability [29,33]. In addition, the MIE measured in experiments strongly depends on the mixture composition (equivalence ratio, dilution), thermal state (pressure and temperature), ignition configuration (geometry of the electrodes, spark gap distance, discharge circuit), and flow conditions (uniform flow, turbulence) [27,29–34,98]. These factors should be considered in future development of ignition theory.

2.2. Effects of low-temperature chemistry

It is well known that chemical reactions occurring at low temperature play an important role in ignition of most hydrocarbon fuels, especially under engine-relevant conditions [44,45]. The LTC may induce a cool flame at certain conditions. It was found that a cool flame can be directly initiated in a dimethyl ether (DME)/air mixture by a hot spot [99] at a proper temperature that only triggers LTC. The premixed cool flame was found to substantially accelerate the subsequent hot flame initiation and propagation, leading to a double-flame structure with coexisting premixed cool and hot flames [99]. This indicates that LTC may promote forced ignition.

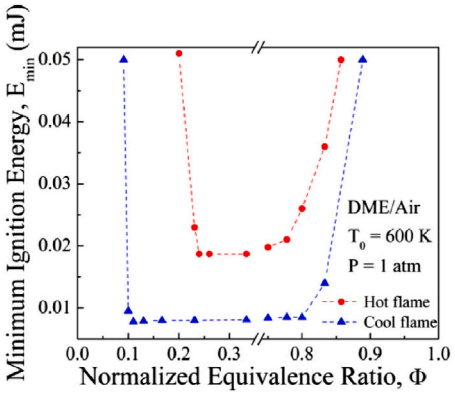

Fig. 6. Comparing the MIE for cool and hot flame ignition in DME/air mixture at 1 atm and 600 K under different normalized equivalence ratios. Reprinted from [100].

Yang and Zhao [100] found that at elevated temperatures, premixed cool flames exhibit a lower MIE and wider flammability limits compared with hot flames. Fig. 6 compares the MIE for cool and hot flames in DME/air over a range of normalized equivalence ratios. The LTC greatly reduces the MIE of cool flames, which is generally less than half of that required for hot flames under the same conditions. Furthermore, LTC markedly extends the lean and rich flammability limits of cool flames, allowing ignition to occur in mixtures where hot flames cannot be initiated. This demonstrates that LTC not only lowers the ignition barrier but also broadens the operational window for premixed combustion [100].

Previous numerical studies [99,100] on cool flame ignition were mostly conducted in 1D, quiescent mixtures, neglecting the influence of flow fields. Wang et al. [101] performed transient 2D simulations of forced ignition in a laminar axisymmetric counterflow, considering both low- and high-temperature chemistry. They systematically investigated the effects of ignition energy and strain rate on the initiation of premixed cool and hot flames. They found that the strain rate strongly affects flame kernel quenching and the transition from cool to hot flame.

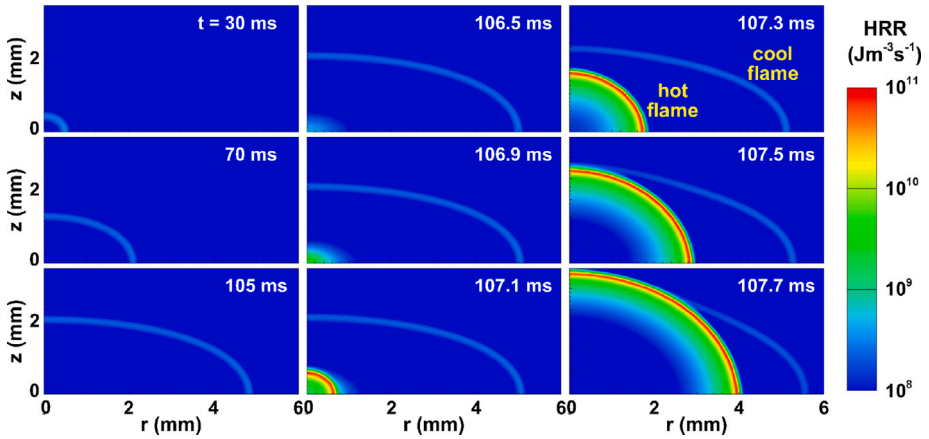

Fig. 7. Temporal evolution of the heat release rate for the case with the strain rate of $a_g = 20\ s^{-1}$ and the ignition energy of $E_{ign} = 0.825$ mJ. Reprinted from [101].

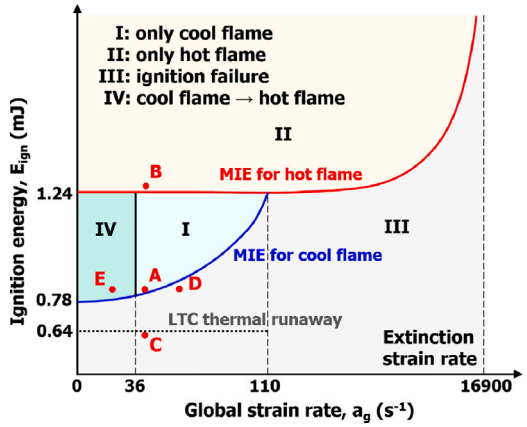

Fig. 8. Ignition regime diagram for DME/air mixture in a counterflow. Reprinted from [101].

Fig. 7 illustrates the ignition process at a low global strain rate of 20 s^{-1}. First, a cool flame kernel forms and expands outward. Because the strain rate is low, the intermediate species produced by the cool flame have sufficient residence time to trigger high-temperature chemistry. Consequently, a hot flame kernel appears near the stagnation point at around $t = 107.1$ ms. The hot flame, with a heat release rate about two orders of magnitude higher than that of the cool flame, propagates rapidly outward and eventually overtakes the leading cool flame, forming a double-flame structure (Fig. 7). Eventually, the cool flame disappears and only the hot flame remains.

Fig. 8 presents a regime diagram with four distinct regions for forced ignition behavior in the counterflow: (I) only cool flame (low to moderate strain rate, moderate ignition energy), (II) only hot flame (high ignition energy), (III) ignition failure (insufficient ignition energy or excessive strain rate leading to kernel quenching), and (IV) transition from cool to hot flame (low strain rate, where the cool flame first appears and later triggers a hot flame) [101]. It clearly demonstrates that the ignition energy primarily controls whether low- or high-temperature chemistry thermal runaway occurs, while the strain rate mainly determines whether the kernel survives or quenches, and whether a cool flame can transition to a hot flame. Besides strain rate, the heat loss was also found to affect the transition from cool flame to hot flame in a channel [102].

The study of forced ignition of cool flames in the premixed system was also extended to non-premixed systems including mixing layer [103] and non-premixed counterflow [104,105]. Wang et al. [104] investigated the forced ignition of cool, warm, and hot flames in a laminar, axisymmetric, non-premixed counterflow of dimethyl ether (DME) versus air using 2D transient simulations. The effects of strain rate and ignition energy on the ignition processes as well as cool and hot flame transitions were systematically examined, and six distinct ignition regimes were identified in the plane of ignition energy versus strain rate [104]. The MIE for cool and hot flames was found to exhibit a non-monotonic dependence on strain rate due to competing effects of mixture reactivity and heat loss. These results provide insights into the flow-affected multi-stage ignition of cool and warm flames in non-premixed systems.

The above results indicate that LTC can reduce the MIE and extends the flammability range for DME and n-heptane. Note that the outcome depends on fuel, temperature, strain rate, residence time, heat loss, pressure, and the competition between cool-flame chemistry and transport, which needs to be explored in future studies. Besides, LTC enables cool flame ignition at lower energies, and under low strain rates, a cool flame can transition to a hot flame, forming double-flame structures.

However, current understanding relies almost entirely on numerical simulations. Theoretical models capturing LTC effects on forced ignition are still lacking, and experimental validation remains scarce. More systematic studies are needed to develop predictive theories and benchmark experiments.

2.3. Effects of imposed flow

Compared to ignition in quiescent premixed mixtures, forced ignition in flowing/turbulent premixed reactants is generally more difficult because the deposited energy dissipates more rapidly [28,32–34]. Many studies (e.g., [106–111]) found that the imposed laminar flow strongly affects the flame kernel development and MIE.

Lefkowitz and Ombrello [112] experimentally investigated nanosecond pulsed high-frequency discharges (NPHFD) for igniting flowing methane-air mixtures. They identified three inter-pulse coupling regimes based on the pulse repetition frequency, illustrated in Fig. 9. In the fully-coupled regime (shortest inter-pulse time, $\tau \leq 2 \times 10^{-5}$ s), successive pulses deposit energy into a small volume, producing a single large ignition kernel with ignition probability of 1. The partially-coupled regime (intermediate τ) leads to elongated kernels where only local ignition occurs, resulting in the lowest ignition probability. In the decoupled regime (longest τ), pulses act independently, creating multiple non-interacting kernels; ignition probability becomes the product of pulse number and single-pulse probability. These three inter-pulse coupling regimes were further interpreted by Lefkowitz and coworkers [113–116]. However, a quantitative theoretical framework that can predict the transition among these three coupling regimes and the corresponding ignition probabilities is still lacking, and the underlying mechanisms remain to be fully elucidated.

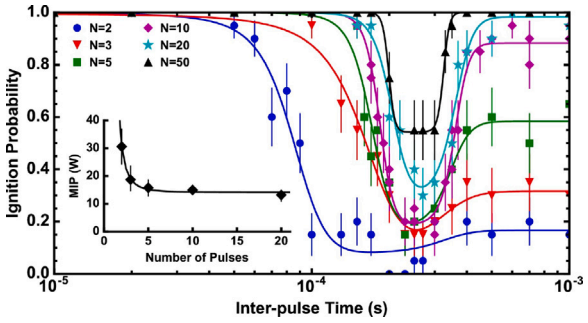

Fig. 9. Ignition probability versus inter-pulse time τ for various numbers of pulses N. The flowing mixture is CH_4/air ($\phi = 0.6$) with $U = 10$ m/s. The inset shows the minimum ignition power as a function of the pulse count. Reprinted from [112].

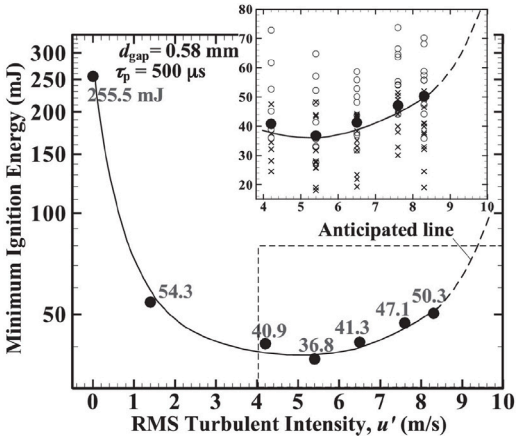

Fig. 10. Minimum ignition energy versus turbulence intensity u' for H_2/air mixture ($\phi = 5.1$, $Le \approx 2.3$) at electrode gap of $d_{gap} = 0.58$ mm. Reprinted from [47].

Besides laminar flow, the effects of turbulent flow on forced ignition were reviewed by Mastorakos [28,32] and Shy [33]. In typical conditions, turbulence hinders ignition by accelerating the dissipation of the energy deposited for kernel development and thereby enhancing heat loss. However, recent experiments reported a counterintuitive phenomenon known as turbulence-facilitated ignition (TFI) in mixtures with large Lewis numbers [46,47].

Fig. 10 illustrates how the MIE of a hydrogen-air mixture with $Le \approx 2.3$ ($\phi = 5.1$) depends on the r.m.s. turbulent fluctuating velocity u' for a small gap of 0.58 mm. The laminar MIE is shown to be extremely high (255.5 mJ) due to severe heat losses and positive curvature stretch that weakens the reaction rate. When weak turbulence is introduced, the turbulent MIE drops sharply, reaching a minimum of 36.8 mJ at $u' = 5.4$ m/s—a clear manifestation of TFI, where turbulence surprisingly makes ignition easier [47]. However, as u' increases beyond this point, the turbulent MIE begins to rise again, indicating that sufficiently intense turbulent dissipation eventually overcomes the beneficial effects of differential diffusion [47].

The mechanisms underlying TFI are still not well understood. A key contradiction is that direct numerical simulations by Uranakara et al. [48] in a turbulent H_2/air mixture with large Le did not reproduce TFI; instead, turbulence created more positively stretched flame fronts, hindering ignition. This discrepancy between experiment and simulation indicates a fundamental gap in understanding how stretch, differential diffusion, heat loss to electrodes, and turbulence dissipation collectively determine ignition outcome. Shy and coworkers [33,47,117] suggested that weak turbulence may blow the kernel away from cold electrodes, reducing conductive heat loss and altering curvature.

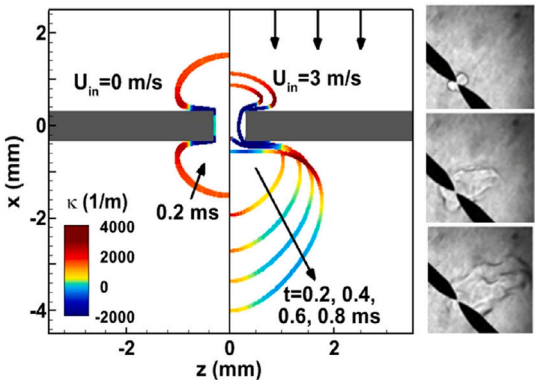

Fig. 11. Temporal development of the reaction front (identified by the $T = 700$ K isosurface) for quiescent (left, $U_{in} = 0$ m/s) and flowing (right, $U_{in} = 3$ m/s) conditions in H_2/air mixture ($\phi = 5.1$, $Le \approx 2.3$). The electrode gap is $d_{gap} = 0.64$ mm. The coloring indicates the local curvature magnitude. The images on the right column are reproduced from Fig. 6 of Ref. [47], which show experimental ignition kernels in turbulent flow by Shy et al. Reprinted from [118].

Recently, Chen et al. [118] have numerically investigated forced ignition in laminar premixed hydrogen/air mixtures with $\phi = 5.1$ and $Le \approx 2.3$, aiming to isolate the effects of heat loss to electrodes and imposed flow – factors that are coupled in turbulent TFI experiments. They considered both quiescent and flowing mixtures. In quiescent mixtures, small electrode gaps ($d_{gap} = 0.64$ mm) cause high positive curvature and severe heat loss to isothermal electrodes, leading to ignition failure despite large ignition energy. Remarkably, imposing a flow normal to the electrodes ($U_{in} = 3$ m/s) reverses the outcome for the case with large Le and small d_{gap}: ignition becomes successful. They called this phenomenon flow-facilitated ignition (FFI) [118], which closely mirrors the experimentally observed TFI [46,47].

Fig. 11 compares the evolution of reaction front in quiescent versus flowing mixtures for the case with a large Lewis number and a small gap distance. In the quiescent case, the flame kernel remains highly curved and attached to the electrodes, while the imposed flow blows the kernel downstream, drastically reducing both the contact area with cold electrodes (thus conductive heat loss) and the positive curvature. This reduction in heat loss greatly promotes the development of the ignition kernel [118]. The competing effects of flow were found: the flow introduces both negative (convective heat loss, hindering autoignition) and positive (reduced heat loss to electrodes and decreased curvature, promoting flame kernel transition) influences. For large Lewis number and small gap distance, the positive effects dominate and the flow-assisted kernel movement becomes the key enabler of TFI [118].

The concept of FFI was further extended by demonstrating numerically its occurrence in low-Lewis-number mixtures under reduced-pressure conditions [119]. While imposed flow was previously believed to promote ignition primarily for mixtures with $Le \gg 1$, this study demonstrated that FFI can also occur in a fuel-lean H_2/air mixture with $Le < 1$ under reduced pressure and small gap distance between electrodes [119]. Fig. 12 shows the ignition kernel evolution for a lean H_2/air mixture ($\phi = 0.4$, $Le \approx 0.43$) at $P = 0.3$ atm, $d_{gap} = 1.44$ mm and fixed $E_{ig} = 0.37$ mJ. Under quiescent conditions ($U_{in} = 0$ m/s), the kernel fails to propagate. At $U_{in} = 6$ m/s, the kernel successfully develops into a self-sustained flame, demonstrating FFI. However, at $U_{in} = 10$ m/s, the kernel fails again due to excessive convective dissipation. This non-monotonic behavior reveals an optimal flow window for FFI even in low-Le mixtures. Generally, FFI is likely to occur in an ignition process that is limited by the difficulty of the flame kernel to grow beyond the critical ignition radius [119].

However, contrary to the simulation [119] reporting FFI at reduced pressure (0.3 atm), the experiments by Mai et al. [120] showed no FFI

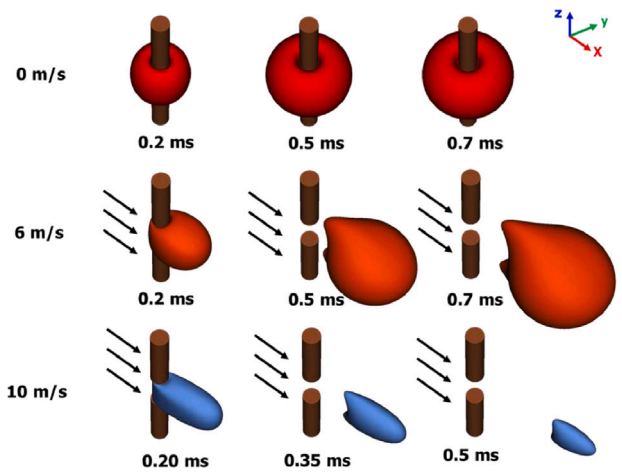

Fig. 12. Time-resolved development of the ignition kernel under quiescent (U_{in} = 0 m/s, shown in red) and flowing conditions with U_{in} = 6 m/s (orange) and U_{in} = 10 m/s (blue) for Cases D–F. The mixture is lean H_2/air (ϕ = 0.4) at P = 0.3 atm, with electrode gap d_{gap} = 1.44 mm and ignition energy E_{ig} = 0.37 mJ. Reprinted from [119].

for $Le \ll 1$ or $Le \approx 1$ at 0.3 atm; instead, the MIE always increases with flow velocity. They found that heat loss alone cannot cause FFI and the role of differential diffusion is crucial. These conflicting results between simulation [119] and experiment [120] indicate that the effects of imposed flow on premixed flame ignition are still not well understood and thereby further research is needed.

Recently, hot-surface ignition has attracted increasing attention due to the critical safety risks posed by accidental ignition of flammable mixtures in aviation and industrial settings [121]. Systematic studies on hot-surface ignition of n-hexane in air have been conducted at Caltech [121–126], and it was found that both LTC and natural convection play important roles in the ignition process. Hot-particle ignition is also of great importance in industrial and fire safety [127,128]. Recent studies [128–139] have revealed that the ignition temperature threshold depends on particle size, convective flow, preferential diffusion, boundary layer development, and LTC. Unlike spark ignition, which features an extremely high hot-spot temperature and rapid energy deposition, hot-surface and hot-particle ignition involve relatively low temperatures and slow heating rates. Consequently, different time scales need to be considered in the theory and modeling of hot-surface and hot-particle ignition.

The above survey indicates that successful ignition depends not only on ignition kernel formation but also on its subsequent propagation. Therefore, in ignition studies, the *flame propagation* of the ignition kernel with high curvature and stretch must be considered [32,34].

3. Flame propagation into autoigniting mixtures

Central ignition in a quiescent mixture can produce spherical flame propagation, widely used to measure laminar flame speed S_u [59–63]. Conventionally, premixed flames are assumed to propagate into a chemically frozen unburned mixture, where no pre-ignition chemistry occurs ahead of the flame front [49–55]. This assumption underpins the classical eigenvalue problem for the laminar flame speed and is valid when the ignition delay time of the unburned gas, τ_i, greatly exceeds the characteristic flame transit time, $\tau_f = \delta_f / S_u$. However, in spark-ignition engines (SIEs), the end-gas is compressed by the advancing flame and piston, reaching high temperatures and pressures. Then τ_i may become comparable to τ_f, causing significant pre-ignition chemistry occurring in end-gas [57,58]. The resulting flame–autoignition interaction yields a rich spectrum of combustion modes—from mildly accelerated flames to violent end-gas autoignition—posing a practically important and scientifically challenging problem [44,57,58]. Therefore, this section focuses on flame propagation into autoigniting mixtures. End-gas autoignition is discussed first, followed by flame–autoignition interaction, and cool flame propagation.

Note that combustion processes controlled solely by autoignition [140] such as MILD combustion [141,142] and autoignited lifted flames [143,144] are not covered here.

3.1. End-gas autoignition

The spontaneous ignition of the end-gas ahead of a propagating flame is commonly considered as the main cause for knock in SIEs [56–58]. Although end-gas autoignition has been extensively studied, the present work concentrates on its fundamental aspects.

Prediction of end-gas autoignition by the Livengood–Wu integral. The occurrence of end-gas autoignition depends on the competition between propagating flame and autoignition in the unburned mixture. If the flame consumes the end-gas before the ignition delay time elapses, no autoignition occurs. Otherwise, autoignition takes place. This competition can be characterized by the Livengood–Wu integral [145]:

$$I = \int \frac{dt}{\tau_i(T, P)} \tag{2}$$

where $\tau_i(T, P)$ denotes the ignition delay time depending on the instantaneous temperature and pressure. Autoignition is expected to occur when the integral I reaches unity.

For a 1D closed chamber of length L, the pressure rise rate is:

$$\frac{dP}{dt} = \frac{S_u}{L}\left(\frac{P}{P_0}\right)^{1/\gamma_u}(P_e - P_0) \tag{3}$$

where P_0 and P_e are the initial and equilibrium pressures, respectively, and γ_u is the specific heat ratio of the unburned mixture. The laminar flame speed S_u depends on both pressure and temperature, often approximated by:

$$S_u = S_0 \left(T_u/T_s\right)^{\alpha} \left(P/P_s\right)^{\beta} \tag{4}$$

with S_0 being the flame speed at reference conditions (T_s, P_s), and α, β constants.

By substituting Eqs. (3) and (4) into Eq. (2) and adopting the isentropic compression assumption to eliminate T_u, i.e., $T_u = T_0 \left(P/P_0\right)^{(1-1/\gamma_u)}$, we obtain the following form of the Livengood–Wu integral:

$$I = \frac{L}{S_0(P_e - P_0)}\left(\frac{T_0}{T_s}\right)^{-\alpha}\left(\frac{P_0}{P_s}\right)^{-\beta} \left[\int \left(\frac{P}{P_0}\right)^{-\frac{1+\alpha(\gamma_u-1)}{\gamma_u}-\beta} \frac{1}{\tau_i(P)} dP\right] \tag{5}$$

The laminar flame speed can be computed at various initial conditions. Curve fitting gives α = 2.058 and β = −0.114 for stoichiometric hydrogen/air mixtures at reference values of T_s = 900 K, P_s = 10 atm, and S_0 = 40.77 m/s. The equilibrium pressure P_e and ignition delay times τ_i under different initial conditions can be obtained from zero-dimensional homogeneous ignition calculations.

As shown in Fig. 13, the critical boundary for autoignition predicted by the Livengood–Wu integral agrees reasonably well with the 1D simulation results. Therefore, the Livengood–Wu integral provides a useful tool for estimating autoignition onset, although its accuracy depends heavily on the fidelity of the models used for laminar flame speed and ignition delay time.

Recently, the Livengood–Wu integral has been extended to large hydrocarbon fuels with multi-stage autoignition [146] and for forced-ignition of premixed flames [147].

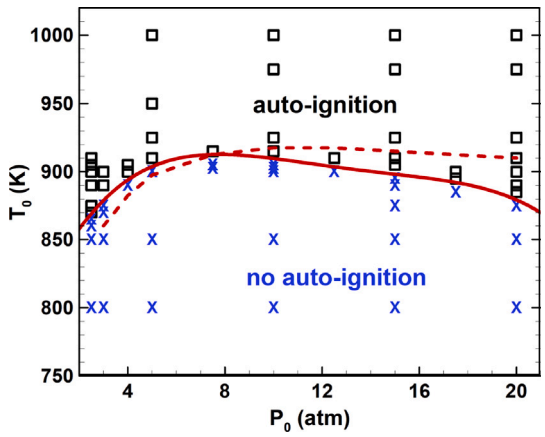

Fig. 13. Critical conditions for autoignition in stoichiometric hydrogen/air mixtures. Symbols represent simulation results: open squares indicate autoignition, crosses indicate no autoignition. The solid line connects the simulation data, while the dashed line corresponds to predictions from the Livengood–Wu integral, Eq. (5).

Asymptotic analysis of end-gas autoignition. While the Livengood–Wu integral offers a practical criterion for estimating the onset of end-gas autoignition, its zero-dimensional nature averages over the spatial structure of the flame and the unburned mixture. To overcome this limitation, Kagan and Sivashinsky [148] performed an asymptotic analysis of the 1D compressible reactive flow equations under the small-Mach-number approximation and developed a hydrodynamic theory of end-gas autoignition.

Kagan and Sivashinsky [148] examined a planar flame traveling in a closed vessel of length L. Within the small-Mach-number framework, acoustic phenomena are eliminated from the leading-order dynamics, and the pressure becomes spatially uniform throughout the vessel, depending only on time. This simplification is justified because deflagrative combustion remains strongly subsonic, yet it preserves the essential compressibility effect arising from the global pressure increase due to thermal expansion. When the ratio of flame thickness to vessel length, $\epsilon = \delta_f / L$, is a small parameter, i.e., $\epsilon \ll 1$ and the activation energy is large, an asymptotic treatment can separate the reactive-diffusive layer (the flame front) from the outer inviscid flow regions. Consequently, the diffusion terms in the governing equations can be neglected in the hydrodynamic theory of end-gas autoignition.

In the analysis of Kagan and Sivashinsky [148], the unburned gas remains spatially uniform in both temperature and composition since diffusive transport is negligible outside the thin reaction zone. For the burned gas region, the entropy conservation equation can be solved analytically, yielding an expression which predicts a non-uniform temperature field within the burned products [148]. By matching the inner and outer solutions across the flame interface and applying integral conservation laws, Kagan and Sivashinsky [148] reduced the full 1D description to a zero-dimensional system of ordinary differential equations which can be solved numerically. The detailed asymptotic analysis can be found in [148].

Kagan and Sivashinsky [148] obtained the following non-dimensional mass burning velocity $\hat{\lambda}$ from the classical Zeldovich–Frank-Kamenetsky asymptotic analysis of the reactive-diffusive layer:

$$\hat{\lambda} = \left(\frac{\hat{T}_-^2}{\hat{C}_+}\right)\left(\frac{\hat{P}}{\hat{T}_-}\right)^{1/2} \exp\left[\frac{N}{2}\left(\frac{\hat{T}_- - 1}{\hat{T}_-}\right)\right] \tag{6}$$

which indicates that when the unburned gas approaches complete consumption through autoignition, the flame speed diverges. This behavior signals a transition from flame propagation to volumetric autoignition in end-gas [148].

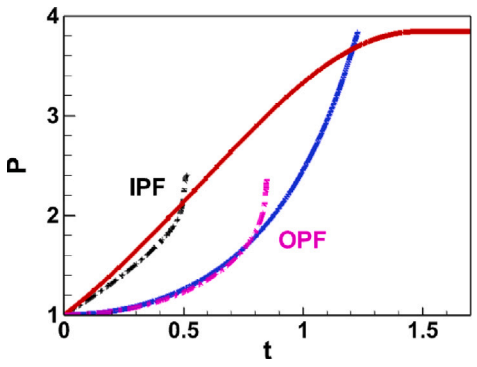

Fig. 14. Temporal evolution of chamber pressure for outwardly and inwardly propagating flames (OPF and IPF). Solid and dashed-dotted lines correspond, respectively, to cases without and with end-gas autoignition. Reprinted from [149].

The analysis of Kagan and Sivashinsky [148] was extended by Yang et al. [149] to compare inwardly and outwardly propagating flames (IPF and OPF). Fig. 14 compares OPF and IPF at two initial temperatures. For low initial temperature without end-gas autoignition (solid lines), OPF exhibits shorter combustion duration than IPF. For high initial temperature with end-gas autoignition (dash-dotted lines), IPF shows shorter duration. Therefore, end-gas autoignition occurs more readily in inwardly propagating flames due to more rapid pressure buildup resulting in higher unburned gas temperature and pressure [149].

It is noted that the small-Mach-number approximation employed by Kagan and Sivashinsky [148] filters out acoustic waves and thereby cannot describe the detailed pressure oscillations characteristic of engine knock or the eventual transition to detonation.

Detailed simulation of end-gas autoignition. While the asymptotic analysis of Kagan and Sivashinsky [148] offers valuable physical insight and helps elucidate the mechanisms underlying end-gas autoignition, it suffers from several inherent limitations when quantitative predictions are required. Chief among these is the use of one-step global reaction kinetics, which cannot accurately capture the complex autoignition behavior of real hydrocarbon fuels, particularly those exhibiting NTC behavior and multi-stage ignition. Moreover, the asymptotic reduction relies on the small-Mach-number approximation that filters out acoustic wave dynamics. Consequently, numerical simulations that incorporate detailed chemical mechanisms and realistic transport properties have been conducted to investigate end-gas autoignition phenomena under engine-relevant conditions [150–158].

Yu and Chen [152] conducted 1D simulations of end-gas autoignition in a closed chamber using stoichiometric hydrogen/air mixtures with the detailed chemistry. Through systematic variation of the initial temperature T_0, initial pressure P_0, and chamber length L, Yu and Chen [152] identified three distinct modes of end-gas combustion: normal flame propagation without autoignition, autoignition without detonation development, and detonation development. Fig. 15 presents the temporal evolution of temperature, pressure, and heat release rate distributions for the case with end-gas autoignition. The time sequence from line #1 to line #9 shows the progression from normal flame propagation through autoignition onset to final consumption of the end-gas. At $t = 323.68$ μs (line #3), autoignition first appears near the right boundary. The autoignition front then propagates leftward (lines #4–#8) and eventually collides with the rightward-propagating flame front at $x \approx 1.52$ cm (line #9). The rapid heat release from autoignition causes the quick pressure rise and strong pressure oscillation [152].

For hydrocarbon fuels with LTC and NTC behavior, multi-stage autoignition in end-gas may occur. Pan et al. [155] simulated flame propagation in a closed chamber filled with n-heptane/air mixtures.

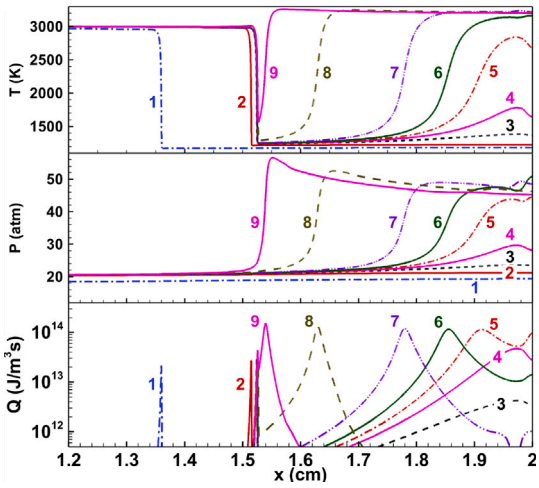

Fig. 15. Time-resolved distributions of temperature, pressure, and heat release rate during end-gas autoignition (stoichiometric H_2/air, L = 2 cm, T_0 = 1000 K, P_0 = 10 atm). The sequential lines correspond to: 1–282.81 μs, 2–320.83 μs, 3–323.68 μs, 4–323.83 μs, 5–323.91 μs, 6–323.99 μs, 7–324.15 μs, 8–324.62 μs, and 9–325.02 μs. Reprinted from [152].

They found that autoignition preferentially occurs upstream of the flame front at lower initial temperatures but shifts to the near-wall region at higher initial temperatures, owing to the competition between the temperature gradient established by flame compression and the NTC behavior of n-heptane.

Besides 1D simulations, multi-dimensional ones have also been used to study end-gas autoignition. For example, Robert et al. [159] performed LES of knocking combustion in a spark-ignition engine and found that knock intensity is proportional to the autoignited end-gas mass at low intensities but increases exponentially at high intensities. Morii et al. [160] conducted 2D DNS of knocking in an n-heptane/O_2/Ar mixture, reproducing experimental pressure and Schlieren images, and capturing cool flame ignition and knock timing. El-Asrag and Ju [161] showed via DNS that 1000 ppm NO enhances DME/air autoignition under HCCI conditions by boosting OH radical pool (10–600 times). Krisman et al. [162] performed DNS of DME autoignition at diesel-relevant conditions, finding that cool flames shorten high-temperature ignition delays, forming kernels at richer mixtures than the homogeneous most-reactive mixture. Wei et al. [163] used LES to investigate combustion in a RCM, revealing that turbulence from the piston crown edge and compressive strain critically affect end-gas autoignition. These studies indicate that LTC is important during end-gas autoignition.

Besides theory and simulation, **experiments** in optical engines and RCMs have been conducted to understand end-gas autoignition. Wang and co-workers [57] have conducted extensive experimental studies of end-gas combustion modes in RCM configurations. Their experiments have revealed a rich variety of end-gas combustion modes. Wei and co-workers [58] have investigated the interaction between turbulent flame propagation and end-gas autoignition in engine-like configurations. Wei et al. [164] demonstrated through combined experimental and numerical studies that the interaction between the propagating flame and shock waves reflected from the chamber walls can trigger autoignition in the end-gas through compression heating. Details on recent progress in experimental studies on end-gas autoignition can be found in recent reviews [57,58].

Despite the above progress, accurate quantitative prediction of end-gas autoignition remains critically important for engine control yet not fully achievable due to many complex factors (e.g., turbulence, multi-stage chemistry, pressure wave interaction), thus demanding further in-depth research.

3.2. Flame–autoignition interaction (FAI)

When the ignition delay time of the unburned gas becomes comparable to the characteristic flame transit time ($\tau_{ig} \sim \tau_f$), pre-flame exothermic reactions progressively alter the thermochemical state ahead of the front. This yields an *autoignition-assisted flame* whose structure, propagation speed, and stability differ qualitatively from a classical deflagration. Autoignition-assisted flames might appear in ICEs, gas-turbine engines, and scramjet combustors in which elevated temperature, pressure, or reactivity places the unburned mixture near its autoignition boundary [22,57,58,165,166].

Early evidence of FAI. The recognition that pre-flame chemistry can distort apparent flame speed dates to the pioneering simulation by Kaufmann and Roth [167], who showed that burning velocity increases monotonically with the reaction progress of the unburned gas in H_2/O_2 and C_2H_6/O_2 mixtures, with the enhancement depending on whether radical or thermal effects dominate. The phenomenon was subsequently characterized in RCMs and high-pressure constant-volume spherical chambers. Assanis et al. [78] found that the influence of autoignition on flame propagation was maximized by igniting the mixtures early in the autoignition process. Xiouris et al. [64] and Movaghar et al. [65] reported that the apparent flame speed increased markedly under conditions approaching the autoignition limit. However, Fan et al. [79] confirmed that, within the NTC regime, the measured flame speed can exceed the true laminar flame speed by up to an order of magnitude. These observations raised a fundamental question: what is the intrinsic speed of a flame whose unburned gas is no longer chemically frozen?

Habisreuther et al. [168] addressed this question for single-stage fuels by computing the structure of premixed methane/air flames at unburned temperatures up to 1450 K using detailed chemistry. Their transport-budget analysis revealed a progressive transition: as the unburned gas temperature approaches the autoignition limit, the preheat zone begins to release heat, the classical eigenvalue structure weakens, and the maximum flame temperature can exceed the adiabatic equilibrium value. Martz et al. [169,170] introduced the time-scale ratio τ_{flame}/τ_{chem} as a quantitative diagnostic for identifying the deflagration-to-spontaneous-ignition transition in iso-octane/air mixtures, establishing the methodology later adopted by Pan et al. [154,171,172]. Building on these foundations, Sankaran [173] used 1D steady-state computations to define a *reference flame speed* S_R in autoigniting H_2/air, showing that even deep in the spontaneous-propagation regime, molecular diffusion contributes a residual speed of ~2 m/s. Krisman et al. [174,175] formalized and extended this framework for two-stage ignition fuels (e.g., n-heptane, DME) and identified two distinct reference flame speeds—one for the cool flame and one for the hot flame—each corresponding to a premixed deflagration.

Experimental characterization of FAI. Different experimental setups have been designed to study flame propagation in autoigniting mixtures. Egolfopoulos and coworkers [64–69] designed a high-pressure, high-temperature spherical chamber and conducted a series of experimental and numerical investigations on flame propagation under engine-relevant conditions using the confined spherically expanding flame (CSEF) method. For example, Lawson et al. [66] demonstrated that CSEF-generated isentropic compression can induce two-stage ignition in dimethyl-ether mixtures, capturing low-temperature chemistry and defining characteristic ignition delay times with high repeatability. Subsequently, they quantified the effects of end-gas reactivity on primary reference fuels blended with ethanol [67], showing that ethanol addition increases ignition delay times and that kinetic model discrepancies grow with fuel octane number.

To isolate flame propagation from far-field autoignition, Hanson and co-workers developed the "Constrained Reaction Volume" (CRV) shock-tube technique [70–77]. Susa and Hanson [74] used schlieren and OH* imaging to visualize the transition from near-wall to distributed spontaneous ignition as post-shock temperature decreases,

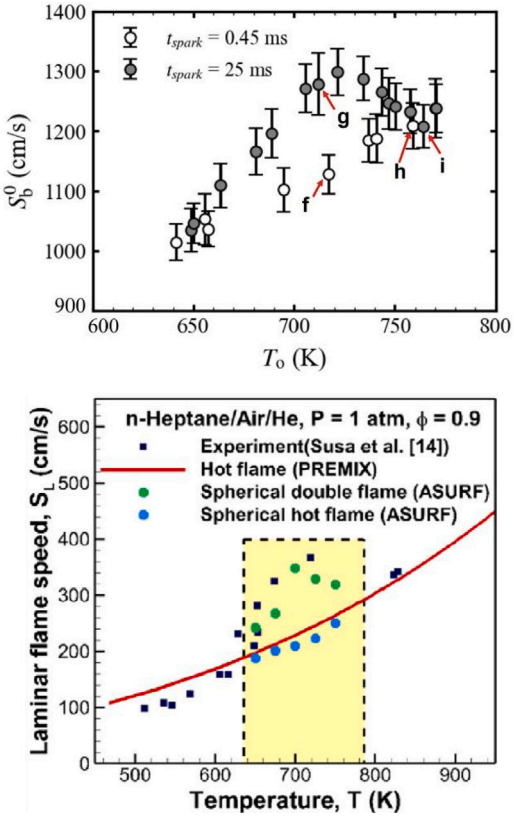

Fig. 16. Non-monotonic temperature dependence of flame speed under autoignitive conditions. Upper: measured S_b^0 of stoichiometric n-heptane-oxygen-argon mixture at two spark timings, showing ~24% enhancement in the NTC window when first-stage autoignition precedes ignition [76]. Bottom: simulated S_L vs. temperature for hot (blue) and double (green) flames with shock-tube data (squares). Reprinted from [177].

confirming a true deflagration at lower temperatures. Combining CRV with laser-induced spark, Ferris et al. [70] established a non-intrusive method for measuring laminar flame speeds above 1000 K. Using this platform, The Hanson group measured flame speeds for n-heptane, iso-octane, propane, and DME [71,72,75,77]. Susa et al. [71,72] provided the first experimental evidence of a negative temperature dependence of iso-octane burning velocity within the NTC window: flame speed decreases with increasing temperature, directly showing that suppressed low-temperature radical generation weakens the pre-flame radical pool. Yang et al. [176] attributed part of this anomaly to thermal-pyrolysis-induced over-driven flames.

More recently, Zheng et al. [76,77] systematically measured n-heptane and DME flame speeds behind reflected shocks with controlled pre-flame autoignition chemistry. By varying spark timing, they isolated flame speed enhancement as a function of first-stage reaction progress, reporting a ~24% increase near the first-stage autoignition boundary followed by non-monotonic temperature dependence (Fig. 16, upper). This directly confirms that upstream autoignition accelerates the flame. Independent validation came from Goyal and Samimi-Abianeh [178,179] using an RCM-Flame at 616–621 K and 6.85 bar, reporting up to 40% enhancement when cool-flame chemistry is active. Zhang et al. [177] explained this non-monotonic behavior using unsteady spherical flame simulations. They identified three regimes (cool, double, hot) controlled by the ignition Damköhler number. The double flame (trailing hot flame sustained by a leading cool flame) propagates much faster than the hot flame alone, producing the observed non-monotonic S_L–T dependence (Fig. 16, bottom). They also showed that the spherical cool flame has a much lower Markstein length than the

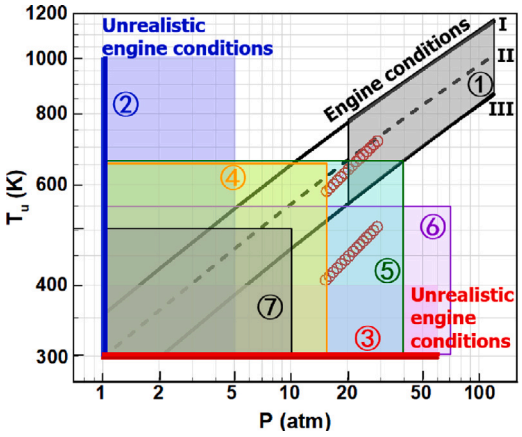

Fig. 17. Mapping of unburned gas temperature against pressure illustrating distinct thermodynamic zones for different existing experiments of laminar flame speed measurement. Reprinted from [180].

hot flame at $T > 600$ K, and proposed a Da_{LTI}-based criterion for accurate flame speed measurement under autoignitive conditions.

Note that many studies have been devoted to measuring laminar flame speed which is one of the most important properties of a flammable mixture [59–63]. Fig. 17 illustrates the unburned gas temperature–pressure landscape relevant to laminar flame speed measurement [180]. Different experimental setups were used to measure laminar flame speeds in different regions. Region 7, characterized by moderate pressure and temperature, has been extensively investigated using various conventional flame configurations [59–63]. Regions 4–6, each covering progressively higher pressures but lower temperatures, have been studied with the constant-volume spherically expanding flame (CVSEF) technique. Region 3, featuring high pressure but near-ambient temperature, relies on a double-chambered apparatus. Region 2, with high temperature but low pressure, has been explored using heated diverging channels and shock tubes. The most challenging region is Region 1, which represents actual engine in-cylinder conditions; currently, it is accessible through the CVSEF technique and RCMs. It is worth noting that in Region 1, the ignition delay of the end-gas can become comparable to the flame transit time, leading to a significant FAI which may considerably affect the accuracy of laminar flame speed measurements.

Flame structure and flame speed scaling. High-fidelity simulations help to reveal the structure of autoignition-assisted flames. Using A-SURF, Faghih et al. [181] studied DME flame propagation into autoigniting mixtures, identifying four stages: initial propagation, first-stage autoignition acceleration, NTC plateau, and second-stage rapid acceleration. Pan et al. [154,171,172] mapped critical transition boundaries between flame-dominated and autoignition-dominated regimes at engine pressures. For NTC fuels, they found a "folded S-curve" in the speed–Damköhler number diagram, with unity speed ratio at cool-flame arrival and hot ignition onset.

Zhang et al. [177,182] provided an analytical model for the autoignition-assisted flame speed. By decomposing the flame into a convection–autoignition zone (from the inlet x_0 to the preheating point x_p), a low-temperature autoignition zone, and a conventional thin reaction–diffusion zone (Fig. 18a), Zhang and Ju [182] derived an analytical expression for the autoignition-assisted flame speed. Using a one-step Arrhenius model in the convection–autoignition zone and the classical large-activation-energy flame speed formula, the preheating temperature T_p is obtained from the ignition Damköhler number $Da_{ig} = \tau_{flow}/\tau_{ig}$ (where $\tau_{flow} = \int_0^{x_f} dx/u(x)$ is the flow residence time) as [182]:

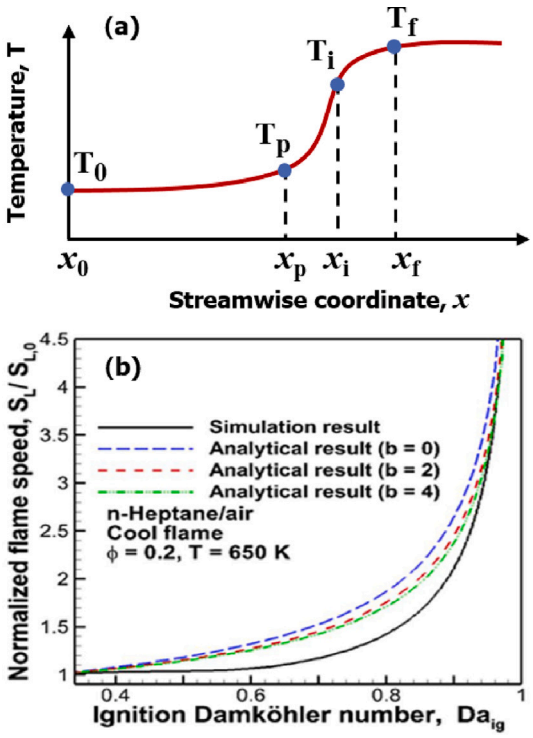

Fig. 18. Analytical model of the autoignition-assisted flame structure (a) and the normalized flame speed $S_L/S_{L,0}$ versus Da_{ig}, showing divergence as $Da_{ig} \to 1$ (b). Reprinted from [182].

$$T_p = \frac{T_a}{\ln\left[(1-\mathrm{Da_{ig}})\, e^{T_a/T_0} + \mathrm{Da_{ig}}\, e^{T_a/T_i}\right]} \tag{7}$$

where $T_a = E_a/R$ is the activation temperature, T_0 the initial temperature, and T_i the ignition temperature. In the limit of large activation energy, we have $T_i \approx T_f$.

The autoignition-assisted flame speed then follows as [182]:

$$S_{L,\mathrm{Da_{ig}}} = S_{L,\mathrm{Da_{ig}}=0}\sqrt{\frac{T_f - T_0}{T_f - T_p}} \tag{8}$$

where $S_{L,\mathrm{Da_{ig}}=0}$ is the flame speed at zero ignition Damköhler number (i.e., with no pre-flame autoignition).

Eqs. (7)–(8) predict that S_L increases nonlinearly with Da_{ig} and diverges as $Da_{ig} \to 1$—the condition at which the flow residence time equals the ignition delay and the entire upstream mixture autoignites before reaching the flame front (Fig. 18b). This divergence, verified against detailed-chemistry simulations using the idealized one-dimensional quasi-steady premixed flame model across multiple equivalence ratios and pressures, provides a first-principles explanation for the dramatic flame speed enhancement observed experimentally. Note that in practice S_L cannot become infinite since it can be regularized by finite domain size, multidimensionality, heat loss, and other factors. Zhang et al. [177] subsequently confirmed this framework through unsteady spherical flame simulations and shock-tube experiments, demonstrating that the analytical S_L–Da_{ig} scaling holds for both cool and hot flames. Gong and Ren [183,184] complemented this theoretical framework with an empirical flame speed decomposition methodology for autoignition-assisted n-heptane/air and jet-fuel/air flames, successfully separating the contributions of deflagration and autoignition to the observed propagation speed.

To examine micro-scale thermodynamic and kinetic feedbacks within the enhanced flame zone, several studies decoupled pre-flame effects. Ansari et al. [185] showed LTC indirectly enhances burning rate by modifying mixture composition and state. Desai et al. [186] analyzed displacement speed budgets for DME/air with thermal stratification; while Soriano and Richardson [187] modeled flame speed for methane/n-heptane blends. Lin et al. [188] found that flame speed enhancement is predominantly thermal while LTC intermediates exert opposing effects.

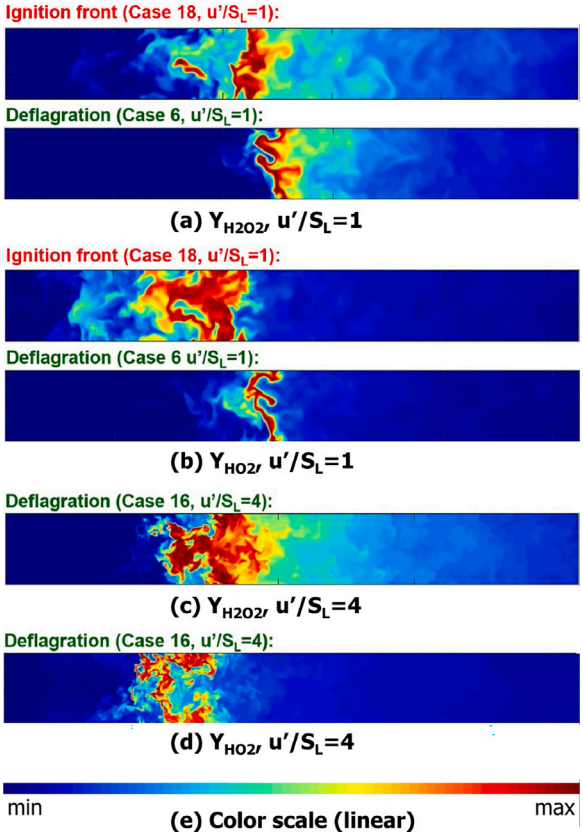

Fig. 19. Structural signatures of turbulent spontaneous ignition versus deflagration indicated by the contours of H_2O_2 and HO_2 mass fraction from DNS of H_2/vitiated air. Reprinted from [196].

Systematic regime mapping by Xiao et al. [189] identified autoignition-assisted cool/hot/double flames and transition regimes for n-heptane/air mixtures as functions of ignition energy and Damköhler number. Akita et al. [190] extended this to stretched flames and showed traditional Markstein-length models fail under autoignitive conditions. Tajima et al. [191] further quantified isochoric reaction progress effects on gasoline-surrogate flame speeds, isolating thermal, pressure, and chemical contributions.

Rencetly, Tsunoda et al. [192] have proposed a theoretical criterion for engine knock onset based on the transition between Zel'dovich–Frank-Kamenetskii (ZFK) mode and Fisher–Kolmogorov–Petrovsky–Piskunov (FKPP) flame propagation regimes, triggered when preheat-zone reactions exceed a threshold. Through linear eigenvalue analysis and re-analysis of DNS data for n-heptane and PRF mixtures, they showned that this transition accurately predicts knock timing, offering a physically grounded alternative to traditional autoignition-based models.

FAI in turbulent flows and engines. Beyond fundamental laminar configurations, the autoignition-assisted flame concept is critical for flame stabilization in modern engineering applications, notably sequential (reheat) gas-turbine combustors, ramjets and scramjets [22,165,166,193–195].

Savard et al. [196] constructed a comprehensive turbulent regime diagram for spontaneous ignition versus deflagration, using over 30

DNS cases of H_2/vitiated air. Contrary to the laminar picture, they showed that turbulence can trigger the transition from spontaneous ignition to deflagration—the opposite of the homogeneous-mixture expectation—through a modified Zel'dovich criterion incorporating turbulent diffusivity. The structural differences between these two regimes are strikingly evident in Fig. 19: in the spontaneous ignition case ($u'/S_L = 1$), H_2O_2 and HO_2 accumulate in broad distributed zones upstream of the reaction front, whereas in the deflagration case ($u'/S_L = 4$), these intermediates are sharply localized at the flame front—a direct visualization of the fundamentally different radical generation mechanisms.

Farjam and Savard [197] extended this framework to real-fuel two-stage ignition by performing DNS of n-dodecane turbulent premixed flames under Engine Combustion Network (ECN) Spray A conditions, demonstrating that both cool-flame and hot-flame fronts can independently undergo spontaneous-ignition-to-deflagration transitions. Aditya et al. [198] performed DNS of flame stabilization in a reheat gas-turbine configuration, showing that autoignition kernels in the windward mixing layer trigger and sequentially assist global flame anchoring. Gruber et al. [199] characterized stable and unstable spontaneous ignition regimes in hydrogen combustion at gas-turbine reheat conditions, demonstrating that compressibility effects are critical for flame stabilization and quantifying the turbulent reaction-front velocity. Collectively, these studies establish that autoignition-assisted flame propagation is not merely a transient phenomenon in ICEs but a fundamental stabilization mechanism in advanced turbulent combustion systems, where a spatially and temporally dynamic coexistence of deflagration, autoignition-assisted propagation, and volumetric autoignition governs the overall combustion behavior.

Several rigorous diagnostic tools have been developed to classify the local combustion mode. The reaction-progress-variable (RPV) framework of Xiao et al. [189] decomposes the total heat release into deflagration and autoignition contributions via the RPV transport equation, demonstrating that the transition between the two modes is sharp and occurs over a narrow range of initial temperatures. Chemical Explosive Mode Analysis (CEMA) [200,201] provides a complementary approach which mathematically distinguishes autoignition from diffusive–reactive fronts, revealing the topological boundaries of autoignition-assisted flames [202,203].

Goldsborough et al. [204] provided a comprehensive review of FAI in engines, surveying early RCM studies on FAI and knock. They also discussed the so-called "mild ignition" (or "weak ignition") observed in shock tubes and RCMs, which introduces substantial scatter in ignition delay time measurements. Mild/weak ignition typically arises from the interplay between volumetric autoignition and a reaction front [204–209]. In shock tubes, the reaction front might be initiated by a localized hot spot produced by shock-boundary interaction (e.g., [210,211]). In RCMs, the reaction front might be initiated by thermal inhomogeneities [204].

In summary, when pre-flame chemistry becomes significant ($\mathrm{Da_{ig}} \sim O(1)$), the classical frozen-mixture flame picture breaks down. The flame speed increases nonlinearly with $\mathrm{Da_{ig}}$ and eventually the entire upstream mixture autoignites. Shock-tube and RCM experiments confirm this enhancement and reveal non-monotonic temperature dependence for NTC fuels. DNS further demonstrates that the spontaneous-ignition-to-deflagration transition can be reversed by turbulence, challenging laminar-based regime criteria. Despite these advances, a unified theoretical framework that quantitatively couples flame propagation with multi-stage autoignition across laminar and turbulent conditions remains to be developed.

3.3. Cool flame propagation

Section 3.2 mainly treats pre-flame chemistry as spatially uniform autoignition. However, for fuels such as n-heptane, DME and n-dodecane, LTC sustains an independently propagating cool flame—an active front that reshapes upstream conditions before the hot flame arrives. Cool flames are driven by first-stage autoignition with ignition delay $\tau_{\mathrm{ig},1}$ short relative to the flame transit time, yielding a large ignition Damköhler number $\mathrm{Da_{ig}} = \tau_f/\tau_{\mathrm{ig},1}$. Thus autoignition–flame coupling is inherent to cool flame propagation, unlike hot flames where such coupling requires extreme thermodynamic conditions (Section 3.2).

This section first examines cool flame propagation governed by LTC, then discusses how the cool flame alters the upstream conditions encountered by the trailing hot flame—a perspective inaccessible from the uniform autoignition framework of Section 3.2. For broader aspects of cool flame dynamics and chemistry, see reviews by Ju et al. [44,45].

Characteristics of premixed cool flames. Cool flames, sustained by LTC with low heat release rate and weak thermal expansion, exhibit fundamentally different propagation from hot flames. Yang and Zhao [100] found that premixed cool flames always decelerate with increasing stretch rate (positive Markstein number), unlike hot flames whose stretch response depends on ϕ and Le. Wang et al. [103] showed that the density-weighted displacement speed S_d^* of a DME/air cool flame varies linearly with Karlovitz number. The unstretched cool flame speed increases with initial temperature but is nearly pressure-insensitive, reflecting the weak pressure dependence of $\tau_{\mathrm{ig},1}$.

The large $\mathrm{Da_{ig}}$ of cool flames makes autoignition–flame competition always significant. Zhang and Ju [182] computed n-heptane/air cool/warm flame structures and speeds over 650–1000 K, 1–20 atm, ϕ = 0.2–20. Cool flame speed increases nonlinearly with $\mathrm{Da_{ig}}$; at $\phi = 0.2$, it can exceed the hot flame speed near the NTC region. The cool-to-warm flame transition (a double-flame structure) occurs when ketohydroperoxide decomposition triggers thermal runaway [99]. At the upper NTC end (~960 K at elevated pressures), warm flames become pure hot flames [182].

Wang et al. [212] simulated spherically expanding DME/air cool flames under gravity using 2D DNS. With propagation speeds < 20 cm/s and a small density ratio, buoyancy effects are strong: at $S_b^0 < 8$ cm/s, natural-convection vortices deform the flame into a mushroom shape. The volume-based equivalent radius $R_{eq,V}$ reliably extracts the unstretched flame speed from distorted shapes, enabling future terrestrial experiments [212].

Effects of cool flame on subsequent hot flame. The preceding paragraph established the intrinsic propagation properties of cool flames. A key consequence for this review is that the cool flame, as a moving front, creates spatially non-uniform upstream conditions for the trailing hot flame—fundamentally different from the uniform autoignition in Section 3.2. In the double-flame configuration, the hot flame no longer propagates into a frozen or uniformly pre-reacted mixture, but instead enters a field of partially oxidized intermediates whose composition and reactivity are imprinted by the cool flame's own dynamics.

Fig. 20 compares the transient behavior of flames initiated by hot spots at two different temperatures. For T_H = 800 K (insufficient to directly trigger high-temperature chemistry), a premixed cool flame first propagates outward (OA in Fig. 20). Later, a hot flame ignites at the center and travels behind the cool flame (HB in Fig. 20). Owing to partial fuel consumption and the temperature rise induced by the cool flame, the trailing hot flame moves significantly faster than a single hot flame (OC in Fig. 20) started at T_H = 1200 K. Eventually, the hot flame catches up and overtakes the cool flame, after which its speed relaxes to the normal hot flame speed. The cool flame itself maintains a nearly constant propagation speed before being overtaken. In contrast, when T_H = 1200 K, only a single hot flame is observed from the beginning, with no cool flame formation. The above results indicate that the premixed cool flame can substantially accelerate the subsequent hot flame initiation and propagation, leading to a double-flame structure with coexisting premixed cool and hot flames [99].

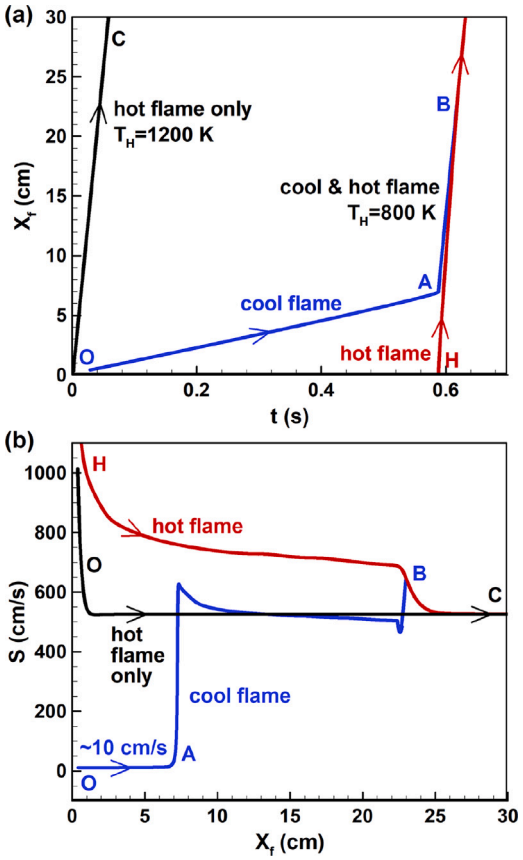

Fig. 20. Evolution of (a) flame front position and (b) flame propagation speed for cool and hot flames initiated by different hot-spot temperatures (T_H = 800 K or 1200 K) in a DME/air mixture. Reprinted from [99].

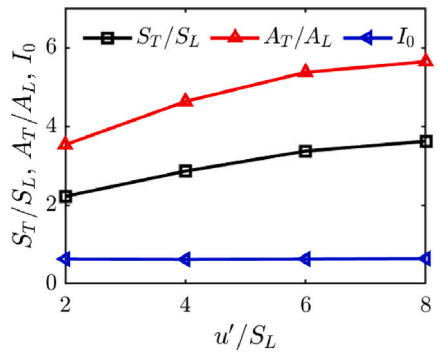

Fig. 21. Time-averaged S_T/S_L, A_T/A_L, and stretching factor I_0 versus u'/S_L for turbulent premixed cool flames. Reprinted from [218].

Savard et al. [213] showed that in 1D simulations of cool flames under NTC conditions, diffusion within the cool flame zone reduces fuel conversion relative to homogeneous autoignition. Thus, the hot flame propagating into post-cool-flame products encounters a less reactive mixture, and its speed is significantly lower than predictions based on homogeneous chemistry alone. This diffusion-mediated "reactivity discount" means the cool flame's propagation mode governs downstream hot flame behavior.

The cool flame's spatial imprint becomes more complex with non-uniform upstream mixtures. Wang et al. [214] found that stratification with increasing ϕ in the propagation direction promotes cool flame propagation, while decreasing ϕ suppresses it—opposite to stratified methane hot flames [215]. A scaling law based on the stratification Damköhler number Da_S collapses the data. In mixing layers, cool flames propagate preferentially from lean to rich via reaction–diffusion, redirecting hot ignition. Krisman et al. [162] showed that a cool flame from the lean DME/air mixture accelerates autoignition in the rich region, forming multi-armed structures. Borghesi et al. [216] found similar behavior in an n-dodecane/air jet. Wang et al. [103] observed a five-armed (penta-brachial) flame with cool, warm, and hot branches in a DME/air mixing layer—an LTC extension of the classical triple flame.

In multi-dimensional geometries, hydrodynamic–chemistry coupling adds further non-uniformity. Zhang et al. [217] performed 2D simulations of laser-induced ignition in n-heptane/O_2/inert mixtures (700 K, 1 atm) and identified a vortex–radical coupling mechanism: the laser spark generates a vortex pair that transports OH radicals into the low-temperature mixture, triggering a C-shaped cool flame roughly three times faster than homogeneous first-stage ignition. At higher laser energies (~10 mJ), a transient premixed double flame (leading cool flame attached to hot flame) was observed, with propagation speed 25% higher than the pure hot flame speed [217]. These 2D vortex-driven structures create locally non-uniform cool flame products that cannot be captured by 1D models, underscoring that the spatial distribution of the cool flame zone—not just average properties—determines the upstream conditions for the hot flame.

Under turbulent conditions, double-flame coupling becomes more complex. Wang et al. [218] studied turbulent premixed n-C_7H_{16}/O_2/O_3/N_2 cool flames using flame-in-box DNS. The normalized turbulent cool flame speed S_T/S_L increases monotonically with u'/S_L (Fig. 21), driven mainly by flame surface area growth, while the stretching factor I_0 remains nearly constant below unity. S_d is strongly negatively correlated with curvature and insensitive to u'/S_L and ϕ [218]—in sharp contrast to turbulent hot flames. This insensitivity implies that spatial non-uniformity from a turbulent cool flame is governed primarily by area-weighted flame speed, simplifying modeling of upstream conditions for the trailing hot flame.

For two-stage ignition fuels under spray-relevant conditions, Farjam and Savard [197] showed that the cool and hot flames can independently undergo the spontaneous-ignition-to-deflagration transition. In DNS of n-dodecane premixed flames at ECN Spray A conditions (ϕ = 1.3, P = 60 atm, T_u = 813 K), they identified a "split" regime: the cool flame transitions to a deflagration and anchors near the inlet, while the hot flame remains stabilized by spontaneous ignition downstream. When the cool flame is a deflagration, diffusion within its reaction zone reduces product reactivity, increasing second-stage ignition delay by up to 2.5 times relative to the homogeneous value [197]. Thus, the cool flame's propagation mode determines the thermochemical state delivered to the hot flame—a mechanism absent in uniform autoignition.

Finally, shock–cool flame interaction offers a distinct route to autoignition-assisted flame. Fan et al. [219] simulated planar shocks (Ma = 1.1–2.6) impinging on spherical DME/air cool flames at 500 K and 1 atm (Fig. 22). Weak shocks (Ma = 1.1) stretch or extinguish small flames via Richtmyer–Meshkov instability. Moderate shocks (Ma = 1.6–2.1) compress the cool flame zone enough to activate intermediate-temperature chemistry, producing a cool–warm coexisting flame that relaxes back to a cool flame (Cases 2 and 5 in Fig. 22). Strong shocks (Ma = 2.6) trigger a rapid cool-to-hot transition: heat release rate increases by three orders of magnitude, flame speed jumps from ~0.5 to ~4.5 m/s, and Da rises from ~0.03 to ~5 (Cases 4 and 7 in Fig. 22) [219].

In summary, cool flames introduce a qualitatively new element into flame–autoignition coupling: a self-propagating LTC-governed front that creates spatially non-uniform, partially reacted upstream conditions for the trailing hot flame. This moving-front perspective—absent from the uniform autoignition framework of Section 3.2—reveals mechanisms such as diffusion-mediated reactivity discount, independent cool/hot flame regime transitions, and shock-induced cool-to-hot flame

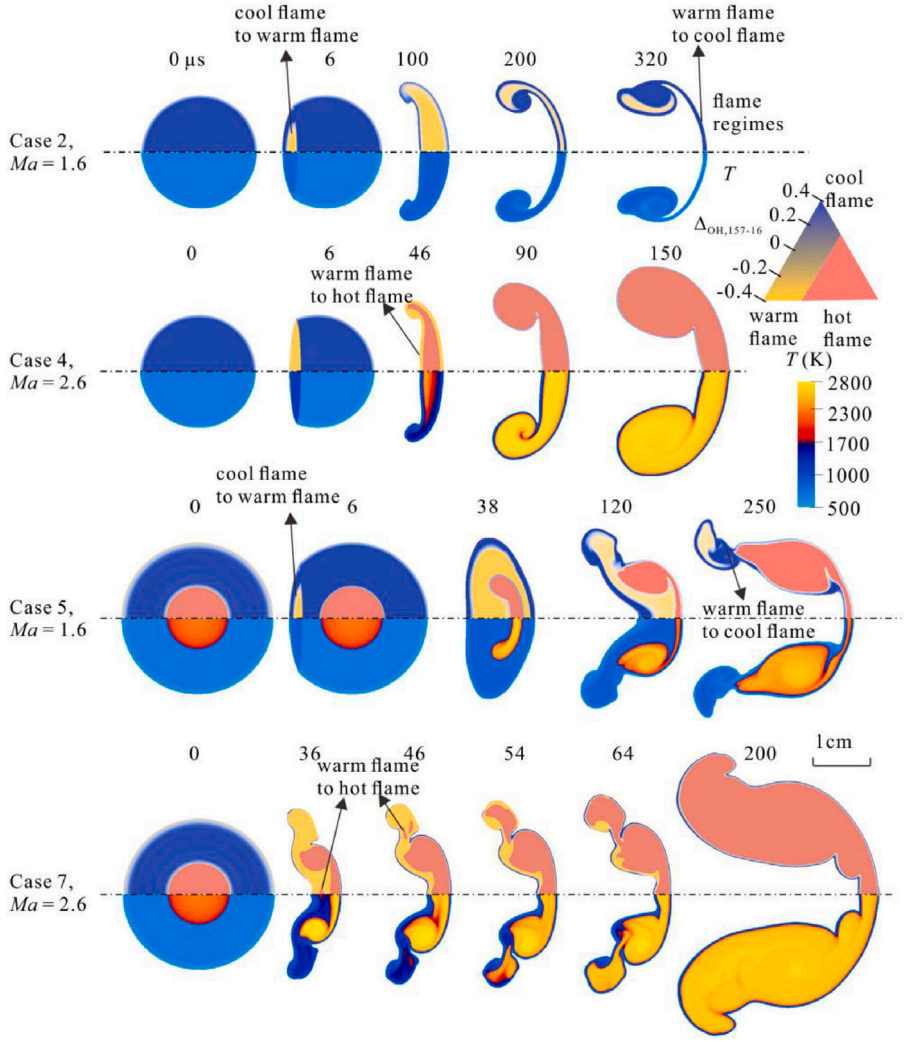

Fig. 22. Flame regime (upper half) and temperature (lower half) contours of shock–cool flame interactions at different Mach numbers. Cases 2 and 5: Ma = 1.6 (small and large initial cool flame); Cases 4 and 7: Ma = 2.6. The color triangle classifies local flame regimes into cool, warm, and hot flames based on the OH reaction indicator and temperature. Reprinted from [219].

conversion. However, most current understanding is based on 1D or simplified 2D configurations with a limited number of NTC fuels. Systematic studies of cool flame propagation and its coupling with hot flames at engine-relevant pressures, in turbulent environments, and for practical multi-component fuels are needed to close the gap between fundamental insights and predictive capability. Under certain conditions, the flame can undergo rapid acceleration and eventually transition into a detonation wave, which is the focus of the next section.

4. Detonation development in autoigniting mixtures

Unlike traditional studies [1–9] on detonation and DDT in chemically frozen mixtures, this section focuses on detonation development in autoigniting mixtures for which the ignition delay time is comparable to the characteristic flame time. Such conditions arise at high temperatures and pressures in spark-ignition engines [57,58], supersonic combustors [22,86,87,165,166], as well as in RCMs and shock tubes.

First, the mechanisms of detonation development in autoigniting mixtures are introduced, and the reactivity gradient theory—which explains how compression waves couple with chemical energy release—is presented. Subsequently, detonation development in a 1D closed tube is analyzed using simplified model configurations. Finally, the transition to detonation in engines is discussed, highlighting the roles of pressure wave reflections, shock focusing, and multi-dimensional interactions.

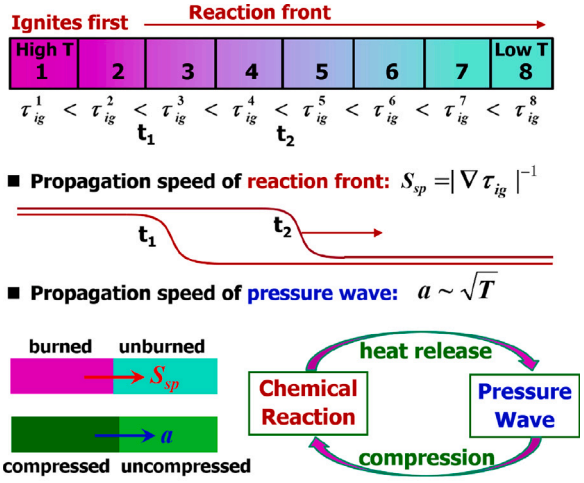

Fig. 23. Schematics of reaction front propagation caused by reactivity gradient and coupling of pressure wave with chemical reaction.

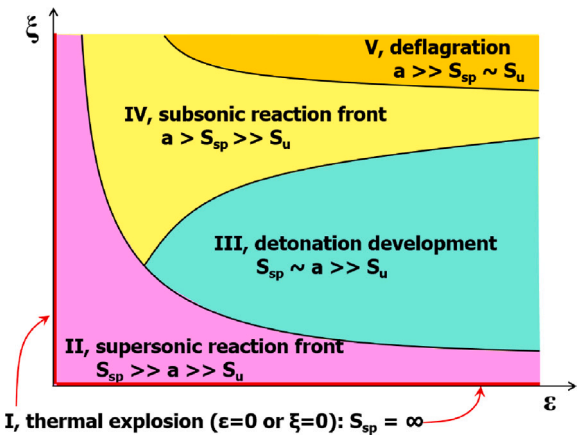

Fig. 24. Schematics of different regimes for five modes of autoignitive reaction front propagation in the ξ–ϵ diagram. Reprinted from [225].

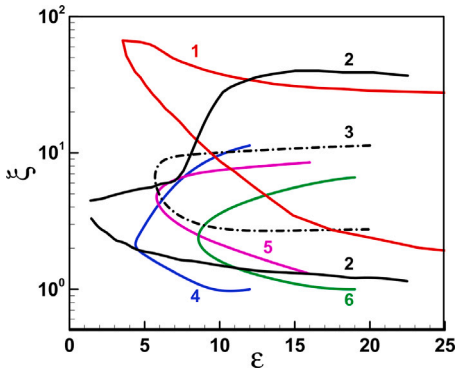

Fig. 25. Detonation development regimes mapped in the ξ–ϵ plane for various fuel/air mixtures. Curve 1: hydrogen/air, ϕ = 1.0, T_0 = 1000 K, P_0 = 20 atm. Curve 2: syngas/air (50% H_2–50% CO), ϕ = 1.0, T_0 = 1000 K, P_0 = 50 atm. Curve 3: *n*-heptane/air, ϕ = 1.0, T_0 = 802 K, P_0 = 40 atm. Curves 4–6: DME/air, ϕ = 1.0, P_0 = 40 atm, with T_0 = 802 K, 982 K, and 1035 K respectively. Reprinted from [225].

4.1. Detonation development induced by reactivity gradient

A key concept for characterizing autoignition and detonation development is the spontaneous ignition front speed introduced by Zel'dovich [82,83]:

$$S_{sp} = \left|\nabla \tau_{ig}\right|^{-1}, \tag{9}$$

which represents the speed at which an autoignition front propagates through a mixture with a spatial gradient of ignition delay time as shown in Fig. 23. The unsteady heat release from chemical reactions generates pressure waves that propagate at the local sound speed, a. These pressure waves can increase the temperature and pressure of unburned gas, thereby accelerating the chemical reactions within it. The enhanced reactions, in turn, produce stronger pressure waves. Consequently, a coherent coupling between chemical reaction and pressure wave occurs when the spontaneous wave speed S_{sp} approaches the sound speed a (i.e., $S_{sp} \approx a$), a condition that may lead to detonation development. This is the essence of the reactivity gradient theory proposed by Zel'dovich [82,83]. Similarly, Lee et al. [1,220] introduced the SWACER (Shock Wave Amplification by Coherent Energy Release) mechanism to explain detonation initiation driven by reactivity gradients. Asymptotic analyses have been performed to better understand detonation development from temperature gradients, revealing the important roles of spontaneous waves, weak detonations, and multi-step chain-branching kinetics [221–224].

Building on Zel'dovich's framework, Bradley and co-workers [84,85] introduced the ξ–ϵ diagram to classify the modes of reaction front propagation from a hot spot:

$$\xi = \frac{a}{S_{sp}}, \qquad \epsilon = \frac{r_{hs}/a}{\tau_e}, \tag{10}$$

where r_{hs} is the hot-spot radius and τ_e is the excitation time (the time interval from 5% to 100% of peak heat release). ξ is proportional to the temperature gradient in the hot spot and ϵ is the ratio of acoustic time to heat release time.

In the ξ–ϵ diagram, five modes of autoignitive front propagation are identified based on comparisons among autoignition front speed S_{sp}, sound speed a, and laminar flame speed S_u (Fig. 24) [84,85,225]. For a uniform mixture ($\xi = 0, \epsilon = 0$), homogeneous autoignition occurs and $S_{sp} = \infty$ (Mode I, thermal explosion). For very small reactivity gradient, $S_{sp} \gg a$ (Mode II, supersonic reaction front), which occurs in end-gas autoignition as shown in Fig. 15. When $S_{sp} \sim a$, detonation may develop (Mode III). For larger gradients, $S_{sp} < a$ (Mode IV, subsonic reaction front), also possible during end-gas autoignition. Further increase in the reactivity gradient yields deflagration with $a \gg S_{sp} \sim S_u$ (Mode V).

The "detonation peninsula" [84,85], Mode III in Fig. 24, defines conditions for hot-spot induced detonation. It has been widely used to interpret super-knock in SIEs [57,226–228]. However, it was originally computed for syngas/air mixtures [84,85]. Later studies [225,229–245] systematically examined the effects of initial temperature, pressure, equivalence ratio, dilution (CO_2, N_2), fuel type (hydrogen, methane, DME, n-heptane, iso-octane, PRF blends), low-temperature chemistry, hot-spot size, chamber closure, and wall reflection on the boundaries for detonation development.

Fig. 25 compares the ξ–ϵ diagrams for detonation development across different fuels and thermal conditions. The regimes differ markedly among hydrogen, syngas, *n*-heptane, and DME, indicating a strong fuel dependence. Moreover, for DME, variations in initial temperature (802, 982, and 1035 K) produce distinct regime boundaries: higher T_0 narrows the detonation peninsula, while lower T_0 broadens it. These observations demonstrate that the detonation development regime is not universal; it is sensitive not only to fuel type but also to the specific thermodynamic state (temperature and pressure) of the unburned mixture. Consequently, predictions of engine knock or super-knock must employ regime diagrams derived for the exact fuel and operating conditions of interest.

Most of these studies [84,85,225,229–245] used 1D simulations without turbulence. Recently, Robert et al. [246] have employed LES of a turbocharged SIE to investigate DDT induced super-knock. They found that for late spark timings, isolated autoignition spots produce weak pressure waves that do not couple with the reaction front, causing moderate knock. For very early timings (mimicking pre-ignition), pressure waves become strong enough to locally raise fresh-gas temperature, drastically reducing autoignition delay. This mutual reinforcement produces a self-sustained reactive front with propagation speeds near Chapman-Jouguet velocity – clear evidence of DDT. A local detonation indicator based on Bradley's ξ–ϵ diagram [84,85] was shown to successfully predict DDT location and timing [246].

Wei et al. [163] performed 1D LEM simulations using time-varying pressure profiles from experiments, revealing a mutual reinforcement between pressure waves and autoignition fronts that induces DDT and super-knock. Similar behaviors were reported in LES of a downsized SI engine by Zhong et al. [247]. Zhang et al. [248] conducted 2D DNS and showed that rapid turbulent mixing can suppress autoignition-to-detonation transition, consistent with earlier findings; larger turbulent mixing length scales weaken knock intensity by creating broader preheated regions ahead of detonation waves. Luong and co-workers [249–251] performed 2D and 3D DNS on the effects of turbulence velocity and temperature fluctuations. Increasing the most energetic length

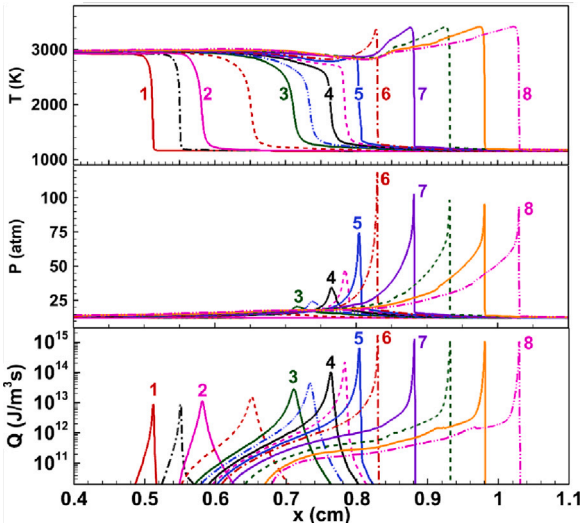

Fig. 26. Time-resolved distributions of temperature, pressure, and heat release rate for Case 5 (stoichiometric hydrogen/air, L = 2 cm, T_0 = 1100 K, P_0 = 10 atm). Curves 1 to 8 correspond to t = 75.00, 83.01, 86.00, 86.50, 86.76, 86.88, 87.11, and 87.81 μs. Reprinted from [152].

scale of temperature or energy enhances detonation propensity by providing a longer run-up distance. Intense turbulent mixing distributes temperature inhomogeneities over wider scales, supporting detonation waves and increasing detonation likelihood. However, very high turbulence intensity with short mixing timescales reduces super-knock intensity due to finer, broken-up detonation structures.

Despite the progress discussed above, there is still a significant challenge in applying Bradley's diagram ξ– ϵ to predict the development of detonations in practical engines, where complex turbulent flows and real multi-component fuels are involved. Bridging the gap between idealized theoretical criteria and realistic engine conditions requires further research, particularly on the coupled effects of turbulent flow, fuel chemistry, and thermal inhomogeneities.

4.2. Detonation development in a 1D closed tube

In order to eliminate disturbances from complex flow fields, wall boundary layers, and heat losses, the study of detonation development can be conducted in a 1D closed tube. This simplified configuration isolates the essential coupling between autoignition and pressure waves, enabling a deeper understanding of the physicochemical mechanisms by which end-gas autoignition leads to detonation.

As mentioned in Section 3.1, Yu and Chen [152] performed detailed 1D simulations for autoignition and detonation development in a stoichiometric hydrogen/air mixture. Among their cases, Case 5 (L = 2 cm, T_0 = 1100 K, P_0 = 10 atm) clearly exhibits DDT and serves as a representative example for understanding the mechanism of detonation development in autoigniting end-gas.

Fig. 26 shows the temporal evolution of temperature, pressure, and heat release rate distributions for Case 5 with detonation development. At t = 75 μs, the flame propagates rightward at a speed about 70 m/s, and the end-gas temperature and pressure increase slowly due to adiabatic compression. However, after $t \approx$ 80 μs, a distinct negative temperature gradient appears upstream of the preheat zone (see Fig. 14b in [152]). This negative gradient implies a spatial variation of reactivity in the end-gas — the gas closer to the flame is hotter and has a shorter ignition delay. When a pressure pulse generated by local heat release propagates downstream, it further compresses the not-yet-autoignited end-gas, raising its temperature and drastically shortening its ignition delay [152]. A positive feedback loop is thus established: the pressure wave enhances chemical reaction, and the heat release further strengthens the pressure wave. From curve 2 to curve 6 in Fig. 26, the peak pressure jumps from about 20 atm to 130 atm, and the peak heat release rate increases by several orders of magnitude. This stage corresponds to a violent acceleration of the reaction front, whose propagation speed rises from an initial 70 m/s to 2233 m/s, eventually forming an overdriven detonation wave around $t \approx$ 87 μs that approaches the C-J speed of 1960 m/s. The close-up in pressure profiles further reveals that just before detonation formation, the pressure wave has already advanced ahead of the reaction front, but because the end-gas is highly reactive, the compressed gas ignites almost immediately upon arrival of the shock wave, enabling strong coupling between the pressure wave and chemical reaction. It is this coupling that causes the reaction front to accelerate beyond the sound speed and spontaneously evolve into a detonation.

Yu and Chen [152] also showed that increasing the initial pressure or the channel length can similarly lead to detonation development, whereas reducing the end-gas reactivity (by lowering initial temperature or pressure) yields only autoignition without detonation. Therefore, sufficient end-gas reactivity, characterized by a strong temperature sensitivity of the ignition delay, is a prerequisite for detonation development.

Recently, Clavin and Chen [252] have developed a theoretical framework to explain the detonation onset observed in the 1D closed tube simulations of Yu and Chen [152]. The analysis focuses on the period immediately before detonation development, when the chemical heat release is still weak but exhibits an extremely high thermal sensitivity due to the chemical reactions at around the crossover temperature.

In the low-Mach-number regime, the end-gas temperature $T_u(t)$ evolves under two contributions: adiabatic compression by the propagating flame and weak exothermic reactions during the induction period [252]. Its governing equation is

$$\frac{\mathrm{d}T_u}{\mathrm{d}t} \approx (\gamma - 1)\frac{Q/c_p}{\tau_e(T_u)} + \frac{q/c_p}{\tau_{ri}(T_u)}, \tag{11}$$

where $\tau_e(T_u) = L/U_L(T_u)$ is the flame transit time, $\tau_{ri}(T_u)$ the induction reaction time scale, Q the total heat release per unit mass, and $q \ll Q$ the small amount of heat released during induction [252]. The thermal sensitivity of the induction reaction is characterized by

$$\beta_i \equiv -\frac{T_u}{\tau_{ri}}\frac{\partial \tau_{ri}}{\partial T_u} \gg b, \tag{12}$$

with b being the thermal sensitivity of the laminar flame speed. Because β_i is large, a slight temperature increase makes the induction term dominate. Once

$$\frac{q/c_p}{\tau_{ri}(T_u)} \gg (\gamma - 1)\frac{Q/c_p}{\tau_e(T_u)}, \tag{13}$$

Eq. (11) reduces to

$$\frac{\mathrm{d}T_u}{\mathrm{d}t} \approx \frac{q/c_p}{\tau_{ri}(T_u)}. \tag{14}$$

Adopting an Arrhenius form for $\tau_{ri}(T_u)$ and introducing the reduced temperature $\theta_i = T_u/T_{ui}$ where T_{ui} is the temperature at which the two heating rates become comparable, the solution of Eq. (14) exhibits a finite-time singularity [252]:

$$\beta_i(\theta_i - 1) = -\ln\left[1 - \frac{t - t_I}{\Delta t_c}\right], \tag{15}$$

with the characteristic time

$$\Delta t_c = \frac{1}{\beta_i}\frac{c_p T_{ui}}{q}\tau_{ri}(T_{ui}). \tag{16}$$

As $t \to t_I + \Delta t_c$, the right-hand side of Eq. (15) diverges, meaning $\theta_i - 1 \sim O(1/\beta_i)$ remains small but the reaction rate $1/\tau_{ri}$ becomes unbounded. This mathematical singularity signals the breakdown of the low-Mach-number approximation [252].

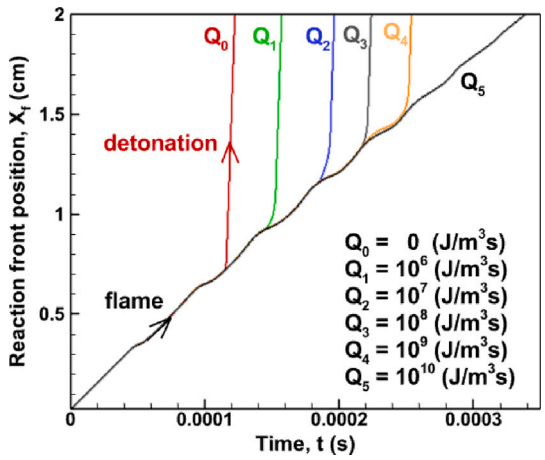

Fig. 27. Time evolution of the reaction front location for various threshold values Q_i of the heat release rate in the end-gas. Reprinted from [252].

The flame acceleration diverges as [252]

$$\frac{1}{U_L}\frac{\partial U_L}{\partial t} \approx \frac{b}{\beta_i}\frac{1}{t_I + \Delta t_c - t}, \tag{17}$$

so that the time scale of flame acceleration becomes shorter than the acoustic time, leading to the formation of shock waves ahead of the flame. The positive feedback between the shock and the highly sensitive induction reactions then blows off the inner flame structure and spontaneously generates a detonation [252].

This theoretical picture is strongly supported by numerical experiments in which the weak heat release in the end-gas is artificially suppressed (by setting a threshold on the heat release rate): the transition to detonation is delayed or even eliminated (Fig. 27). Therefore, Clavin and Chen [252] provided a clear physical framework for understanding detonation development induced by end-gas autoignition.

The mechanism described above differs from Clavin's previous theory [9,253–255] on DDT at the tip of an elongated flame initiated by a spark at the center of a closed vessel and propagating into a cold mixture. In that earlier scenario for frozen mixtures, the transition is driven by the impingement of a backflow on the flame tip; whereas in the present case for autoigniting mixtures, the ultimate acceleration originates from the extreme thermal sensitivity of the induction chemistry in the end-gas itself, without requiring wall reflection or obstacles.

Note that besides detonation development in autoigniting mixtures, many experimental and numerical studies [256–273] have been recently conducted for flame acceleration and DDT in flammable mixtures at normal temperature and pressure in tubes/channels. For example, Yanez and Kuznetsov [260] identified a quasi-stationary "strange wave" as an intermediate stage during DDT, consisting of a strong shock followed by a wrinkled funnel-shaped flame. Such "strange wave" was also observed in experiments using simultaneous two-direction schlieren visualization [261]. The novel two-directional high-speed schlieren technique offers an unprecedented perspective on DDT, capturing three-dimensional flame-shock structures that single-view or one-dimensional approaches cannot resolve. Using this technique, Ballossier et al. [266] revealed that asymmetries dominate flame acceleration while walls and corners play a key role in creating ignition centers, challenging common symmetry assumptions in modeling. The experimental observation was confirmed by recent 3D simulations performed by Alzer et al. [271]. Mejia-Botero et al. [272,273] introduced a flame morphology classification scheme based on fundamental combustion properties, which categorizes flame/shock evolution patterns and detonation onset mechanisms according to morphological characteristics. Using a simple model and asymptotic analysis, Deshaies and Joulin [274] identified a critical flame folding factor beyond which self-similar deflagration solutions cease to exist, leading to thermal runaway and DDT. Based on Deshaies-Joulin theory [274], Sivashinsky and coworkers [275–279] demonstrated that DDT occurs when the flame folding factor exceeds a critical threshold for both planar and spherical geometries.

Recently, studies on the effects of plasma, ozone addition and LTC on DDT and detonation propagation have begun to emerge. For example, plasma-assisted DDT in H_2/O_2 [280,281] and DME/O_2/Ar mixtures [265] have been investigated experimentally and numerically, revealing that coupling between plasma and combustion chemistry helps to accelerate DDT. Recent progress on plasma-assisted detonation can be found in [31,282–284]. As a strong oxidizer and long-lifetime product by plasma, ozone can be introduced to enhance combustion and detonation development [31,285]. Shi et al. [286] experimentally investigated how ozone addition affects detonation limits in small tubes for stoichiometric H_2/O_2 and CH_4/O_2 mixtures. They found that ozone can substantially reduce detonation cell size and delay the onset of spinning detonation, yet it negligibly alters velocity deficits far from the limit. Sun and Chen [287] numerically investigated cellular detonation dynamics in $C_2H_4/O_2/O_3/N_2$ mixtures and found that weak initiation first produces a low-speed single-cellular detonation sustained solely by first-stage reactions, which later transitions to double-cellular structures through vorticity-induced hot spots and second-stage energy release. Besides, ozone has also been found to promote DDT and detonation development [288–293]. Usually, LTC is neglected in detonation studies because of the high post-shock temperatures. However, in autoigniting or highly diluted mixtures, LTC might significantly influence detonation initiation, propagation and quenching [230,231,244,294–297]. Romano et al. [294,295] experimentally investigated how LTC oxidation affects DDT in pentane-oxygen mixtures. They found that ignition during the early cool flame reduces the run-up distance by half due to radicals and peroxides, whereas delayed ignition after the cool flame desensitizes the mixture and increases the run-up distance. Liang et al. [296] examined the effects of LTC on ZND detonation structure in highly CO_2-diluted n-heptane/oxygen mixtures, revealing two-stage energy release with LTC controlling the first stage. However, their simulations yield detonation induction length exceeding 10 cm, making experimental realization of such two-stage detonation challenging. In a brief summary, plasma, ozone addition, and LTC each offer unique kinetic pathways to modulate detonation dynamics. Combining these approaches could enable detonation control. However, complex interaction between chemistry and gas dynamics will be involved and it needs to be explored in future studies.

4.3. Detonation development in engines

In spark-ignition engines, detonation development in autoigniting mixtures results in extremely high pressure as well as pressure rise rate which may damage engine components and reduce thermal efficiency [56–58]. Recently, Wang et al. [57] and Zhou et al. [58] have comprehensively reviewed the fundamental understanding and engineering solutions for detonation development in engines.

Wang et al. [57] extensively employed optical engines and RCMs to experimentally investigate detonation development under engine-like conditions. As shown in Fig. 28, different types of detonation development were observed in their experiments [298–300]. They found that detonation in super-knock is mainly driven by shock wave reflection. Flame propagation from a pre-ignition hotspot compresses the end-gas, raising its pressure and temperature. A local auto-ignition event generates an incident shock wave. Upon reflection at the cylinder wall, the incident and reflected waves interact to form a Mach stem, which further compresses the adjacent unburned mixture. This compression shortens the ignition delay and couples chemical heat release with the pressure wave, a process termed Shock Wave Reflection Induced Detonation (SWRID) [57,301]. The resulting self-sustained

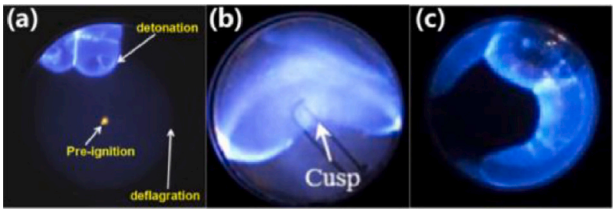

Fig. 28. Different end-gas combustion modes observed in experiments by Wang and coworkers: (a) triple-detonation [298], (b) double-detonation [299] and (c) double-tongue reaction front [300].

detonation propagates at or above the Chapman-Jouguet speed, consistently initiating near the wall. Therefore, detonation development in the specific RCM and engine-like configurations studied by Wang and co-workers [57,301] arises from SWRID.

Yang et al. [302] used 2D simulations with detailed chemistry to investigate end-gas autoignition and detonation development in a closed circular domain, imposing near-wall temperature disturbances of varying amplitude ΔT. The numerical results capture three distinct combustion modes (Fig. 29) that closely resemble the experimental observations of Wang and co-workers (Fig. 28). Fig. 29 shows that for small ΔT, a triple-detonation structure forms, comprising a radial detonation from shock-flame coupling and two circumferential detonations via near-wall shock compression. Moderate ΔT suppresses the radial detonation, yielding a double-detonation structure with two circumferential detonations through near-wall autoignition. Large ΔT prevents detonation entirely; rapid autoignition consumes the end-gas, producing a double-tongue front. These simulations elucidate how temperature disturbance amplitude governs the transition from deflagration to detonation in engines.

Note that, besides ICEs and RCMs, detonation development in autoigniting mixtures provides plausible hypotheses for fast-flame flashback occurring in scramjet engines [86,87]. For instance, Wang et al. [87] examined combustion instabilities in an ethylene-fueled scramjet engine. For injection configurations that create a premixed region upstream of the cavity, the cavity pilot flame periodically reignites the mixture, producing strong flame oscillations as shown in Fig. 30. During flame flashback, the flame accelerates upstream at absolute speeds exceeding 1000 m/s — higher than half the Chapman–Jouguet (CJ) detonation speed. They proposed a DDT-type oscillation cycle [87]: reignition delay, flame acceleration akin to DDT, flash-forward to the injector, then blowoff and recession. Although detonation does not fully develop due to insufficient mixing at the injector, it was hypothesized that local detonation initiation may occur [87]. Recently, Zhao et al. [303] have also attributed flame flashback in a supersonic combustor to a DDT-like process. They found that enhanced injection parameters increase heat release, promoting boundary layer separation and thermal choking. The flame front then accelerates upstream, reaching speeds between CJ detonation and deflagration velocities, supporting a DDT interpretation [303].

As mentioned before, detonation engines including PDEs, RDEs and ODEs have promising applications in advanced propulsion [16–26]. In PDEs [16,17], detonation development usually occurs in cold non-autoigniting mixtures and DDT can be accelerated by a Shchelkin spiral. In RDEs [21,23], detonation development in autoigniting mixtures may occur when fresh reactants mix with hot products. In ODEs [22,24], the mixture ahead of the oblique shock can reach high temperatures such that autoignition occurs before the oblique detonation wave develops. Recently, Yu and coworkers [304,305] have investigated oblique detonation initiation in supersonic reactive flows. They showed that the reactivity-gradient theory of Zel'dovich [82,83] can be used to explain the formation of oblique detonation wave induced by thermal nonuniformity in a supersonic autoigniting mixture.

In summary, this section reviews detonation development in autoigniting mixtures, focusing on the reactivity-gradient mechanism, the spontaneous front speed S_{sp}, and the ξ-ϵ diagram for classifying reaction-front modes. Importantly, in practical engines, ignition kernel formation by forced-ignition, flame propagation and its interaction with autoignition, and the transition to detonation are not isolated processes; they are tightly coupled and must be investigated together. This integrated nature introduces great complexity and poses significant challenges for developing accurate quantitative prediction models essential for engine design.

5. Conclusions

5.1. Summary

This paper reviews the continuous physical chain from forced ignition to flame propagation and finally to detonation development in laminar, premixed, gaseous mixtures.

For forced ignition, theoretical advances reveal that critical ignition radius and minimum ignition energy (MIE) strongly depend on Lewis number, flame stretch, and the unsteady memory effect of energy deposition. Low-temperature chemistry (LTC) can promote ignition by reducing MIE and extending flammability limits, enabling cool flames that may transition to hot flames under low strain rates.

For flame propagation into autoigniting mixtures, when end-gas ignition delay becomes comparable to flame transit time, end-gas autoignition occurs. This can be predicted by the Livengood–Wu integral, asymptotic analysis, and detailed simulations. The resulting flame–autoignition interaction gives rise to autoignition-assisted flames whose speed increases nonlinearly with ignition Damköhler number. Cool flames, driven by LTC, propagate even below the hot flame flammability limit, creating non-uniform upstream conditions that fundamentally alter hot flame behavior.

For transition to detonation, a positive feedback loop between pressure wave and chemical reaction can lead to detonation development via the reactivity-gradient mechanism. In practical engines, such autoignition-induced detonation is responsible for super-knock in SIEs and might also happen in scramjet engines as well as rotating and oblique detonation engines.

Note that forced ignition, flame–autoignition interaction, and detonation transition are tightly linked and should be studied together to advance practical engine design.

5.2. Future research

While significant progress has been made in understanding flame initiation, propagation, and transition to detonation, there are still important challenges that remain to be addressed.

Forced ignition with low-temperature chemistry and flow. Current ignition theories are mostly based on one-step chemistry and quiescent mixtures. Future work should develop ignition theory that incorporates low-temperature chemistry to capture cool flame ignition and its transition to hot flames. The counterintuitive phenomena of flow-facilitated ignition (FFI) and turbulence-facilitated ignition (TFI) remain poorly understood and require combined experimental, numerical, and theoretical efforts to resolve discrepancies between simulations and experiments. Finally, benchmark experiments on forced ignition with high-speed diagnostics are urgently needed for hierarchical validation of ignition theory and modeling.

Autoignition-assisted flame propagation. Accurately predicting flame behavior in autoigniting mixtures remains difficult due to the interplay of turbulence, multi-stage chemistry, and pressure-wave feed-

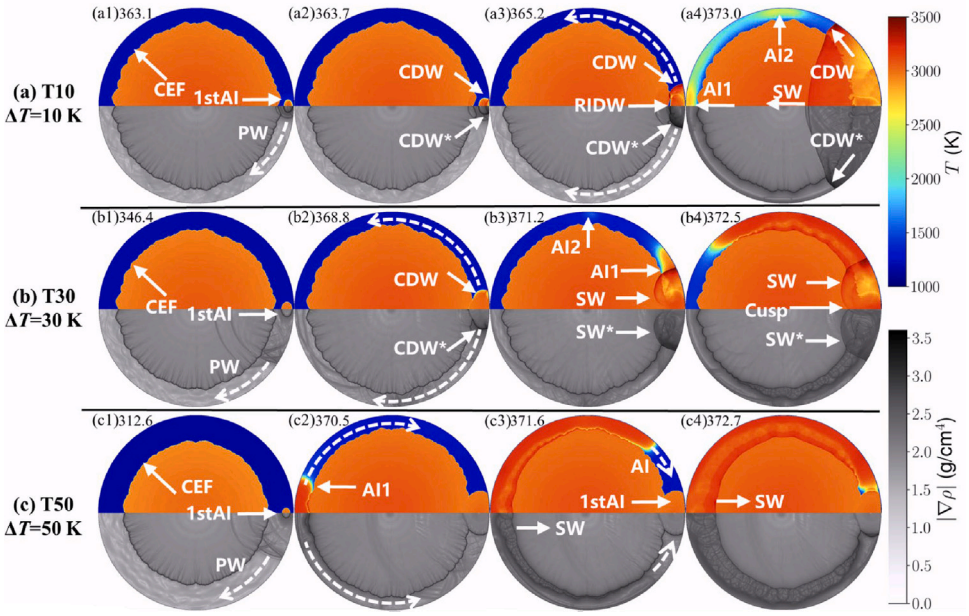

Fig. 29. Contours of temperature (top row) and density gradient (bottom row) at four instants (in the unit of microsecond) during the end-gas combustion in a stoichiometric hydrogen/air mixture for ΔT = 10 K (a), 30 K (b) and 50 K (c). The radius of circular domain is 2 cm. CEF: circular expanding flame; AI: autoignition; CDW: circumferential detonation wave; RIDW: radial detonation wave; SW: shock wave; PW: pressure wave. The symbol '*' denotes that the detonation/shock wave is in the symmetry plane and is not simulated. Reprinted from [302].

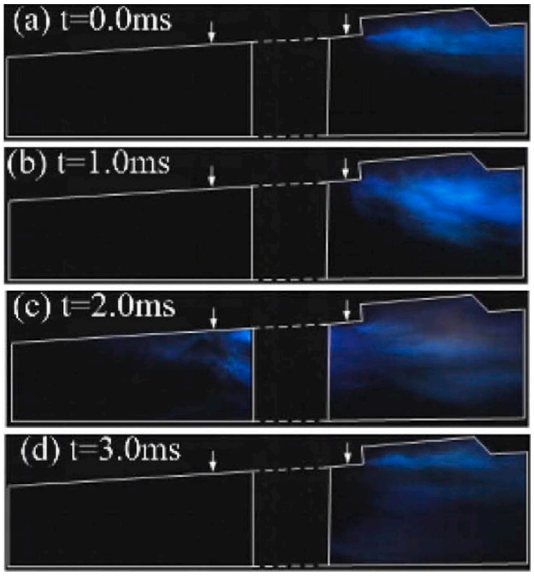

Fig. 30. High-speed luminosity images showing flame oscillations at the cavity-anchored flameholding position for Scheme 5. Reprinted from [87].

back. Reduced-order models based on ignition Damköhler number Da_{ig} should be validated against high-fidelity DNS and advanced optical diagnostics. Furthermore, the current Da_{ig} framework treats upstream autoignition as a lumped effect. Future work should decompose it into its chemical contribution and its thermodynamic contribution, so that mechanism-informed models can replace empirical correlations. The propagation and stability of cool and warm flames at elevated pressures also need systematic characterization, including their stretch response and role in creating non-uniform upstream conditions for hot flames. Beyond passive characterization, an active-design perspective is called for: given a target combustion mode under extreme engine conditions (ultra-lean, ultra-high pressure, or supersonic inflow), can the requisite upstream thermochemical state be reverse-engineered—through fuel blending, thermal stratification, or plasma actuation—to achieve desired combustion organization while avoiding knock or extinction?

Detonation development in autoigniting mixtures. The transition from deflagration to detonation in autoigniting mixtures is a highly nonlinear multi-scale problem. There is presently no accurate quantitative theoretical model for predicting detonation development under realistic engine conditions. Future studies should elucidate the coupled effects of multi-stage autoignition and pressure waves on detonation development. The "detonation peninsula" based on Bradley's ξ–ϵ diagram and the shock-wave-reflection-induced detonation (SWRID) mechanism identified in RCMs offer useful frameworks, but quantitative criteria for detonation onset in engines are still missing. To connect simplified theoretical predictions with real engine environments, additional investigation is needed, especially into the interactions among turbulence, fuel chemistry, and temperature non-uniformities.

CRediT authorship contribution statement

Zheng Chen: Writing – original draft, Writing – review & editing, Investigation, Conceptualization, Funding. **Wang Han:** Writing – original draft, Writing – review & editing, Investigation. **Tianhan Zhang:** Writing – original draft, Writing – review & editing, Investigation.

Declaration of competing interest

The authors declare that they have no known competing financial interests or personal relationships that could have appeared to influence the work reported in this paper.

Acknowledgments

Z.C. wishes to express his sincere gratitude to Professors Osamu Fujita and Venkat Raman as Program Co-Chairs of the 42nd International Combustion Symposium for the invitation to present this Plenary Lecture. Z.C. is deeply grateful to his Ph.D. advisor, Prof. Yiguang Ju at Princeton University, for his invaluable guidance and for introducing him to the wonderful field of flame dynamics. Z.C. also sincerely thanks

Professors Chung K. Law and Frederick Dryer at Princeton University for their insightful guidance and support. Z.C. has greatly benefited from the opportunities to work together with his colleagues at Peking University: Profs. Jian-Ping Wang, Yue Yang, Shengkai Wang, Zhi Chen, Hao Zhao, Haiyang Wang, et al. Z.C. also expresses his gratitude to his collaborators including Profs. Henning Bockhorn, Paul Clavin, Joel Daou, Fokion N. Egolfopoulos, Xiaolong Gou, Fabien Halter, Christian Hasse, Wenjun Kong, Bruno Renou, Arne Scholtissek, Feichi Zhang, Thorsten Zirwes, et al. Most importantly, Z.C. thanks all his current and former students and postdocs, and in particular, Xinyi Chen, Peng Dai, Mahdi Faghih, Zisen Li, Jie Sun, Yan Wang, Yiqing Wang, Yuan Wang, Shumeng Xie, Linlin Yang, Dehai Yu, Hao Yu, Huangwei Zhang, and Weikuo Zhang.

Financial support from the National Natural Science Foundation of China (52425604, 51322602) is acknowledged.

References

[1] J.H.S. Lee, I.O. Moen, The mechanism of transition from deflagration to detonation in vapor cloud explosions, Prog. Energy Combust. Sci. 6 (4) (1980) 359–389.
[2] G.I. Sivashinsky, Some developments in premixed combustion modeling, Proc. Combust. Inst. 29 (2) (2002) 1737–1761.
[3] P. Clavin, Theory of gaseous detonations, Chaos: An Interdiscip. J. Nonlinear Sci. 14 (3) (2004) 825–838.
[4] E.S. Oran, V.N. Gamezo, Origins of the deflagration-to-detonation transition in gas-phase combustion, Combust. Flame 148 (1–2) (2007) 4–47.
[5] J.H.S. Lee, The Detonation Phenomenon, Cambridge University Press, 2008.
[6] G. Ciccarelli, S. Dorofeev, Flame acceleration and transition to detonation in ducts, Prog. Energy Combust. Sci. 34 (4) (2008) 499–550.
[7] S.B. Dorofeev, Flame acceleration and explosion safety applications, Proc. Combust. Inst. 33 (2) (2011) 2161–2175.
[8] P. Clavin, G. Searby, Combustion Waves and Fronts in Flows, Cambridge University Press, 2016.
[9] P. Clavin, Physics of the transition to detonation of gaseous flames, Eur. Phys. J. Plus 140 (2025) 258.
[10] J.X. Wen, E.S. Hecht, R. Mével, Recent advances in combustion science related to hydrogen safety, Prog. Energy Combust. Sci. 107 (2025) 101202.
[11] M.P. Sherman, M. Berman, The possibility of local detonations during degraded-core accidents in the bellefonte nuclear power plant, Nucl. Technol. 81 (1) (1988) 63–77.
[12] W. Breitung, C. Chan, S. Dorofeev, A. Eder, B. Gelfand, M. Heitsch, R. Klein, A. Malliakos, E. Shepherd, E. Studer, et al., Flame acceleration and deflagration-to-detonation transition in nuclear safety, State-of-the-Art Rep. OECD Nucl. Energy Agency, NEA/CSNI/R(2000)7 (2000).
[13] R. Gharari, H. Kazeminejad, N.M. Kojouri, A. Hedayat, A review on hydrogen generation, explosion, and mitigation during severe accidents in light water nuclear reactors, Int. J. Hydrog. Energy 43 (4) (2018) 1939–1965.
[14] G. Chamberlain, E. Oran, A. Pekalski, Detonations in industrial vapour cloud explosions, J. Loss Prev. Process. Ind. 62 (2019) 103918.
[15] S. Hou, Y. Liu, Z. Wang, M. Jing, Y. Zhang, B. Zhang, The potential for deflagration to detonation transition (DDT)-lessons from LPG tanker transportation accident, J. Loss Prev. Process. Ind. 80 (2022) 104902.
[16] G.D. Roy, S.M. Frolov, A.A. Borisov, D.W. Netzer, Pulse detonation propulsion: challenges, current status, and future perspective, Prog. Energy Combust. Sci. 30 (6) (2004) 545–672.
[17] P. Wolanski, Detonative propulsion, Proc. Combust. Inst. 34 (1) (2013) 125–158.
[18] F.K. Lu, E.M. Braun, Rotating detonation wave propulsion: Experimental challenges, modeling, and engine concepts, J. Propuls. Power 30 (5) (2014) 1125–1142.
[19] B.A. Rankin, M.L. Fotia, A.G. Naples, C.A. Stevens, J.L. Hoke, T.A. Kaemming, S.W. Theuerkauf, F.R. Schauer, Overview of performance, application, and analysis of rotating detonation engine technologies, J. Propuls. Power 33 (1) (2017) 131–143.
[20] V. Anand, E. Gutmark, Rotating detonation combustors and their similarities to rocket instabilities, Prog. Energy Combust. Sci. 73 (2019) 182–234.
[21] J.Z. Ma, M.-Y. Luan, Z.-J. Xia, J.-P. Wang, S.-J. Zhang, S.-B. Yao, B. Wang, Recent progress, development trends, and consideration of continuous detonation engines, AIAA J. 58 (12) (2020) 4983–5028.
[22] Q. Liu, D. Baccarella, T. Lee, Review of combustion stabilization for hypersonic airbreathing propulsion, Prog. Aerosp. Sci. 119 (2020) 100636.
[23] V. Raman, S. Prakash, M. Gamba, Nonidealities in rotating detonation engines, Annu. Rev. Fluid Mech. 55 (2023) 639–674.
[24] Z. Jiang, Standing oblique detonation for hypersonic propulsion: A review, Prog. Aerosp. Sci. 143 (2023) 100955.
[25] H. Teng, C. Tian, Y. Zhang, L. Zhou, H.D. Ng, Morphology of oblique detonation waves in a stoichiometric hydrogen-air mixture, J. Fluid Mech. 913 (2021) A1.
[26] J. Sun, P. Yang, Z. Chen, Dynamic interaction patterns of oblique detonation waves with boundary layers in hypersonic reactive flows, Combust. Flame 272 (2025) 113832.
[27] C.K. Law, Combustion Physics, Cambridge University Press, 2010.
[28] E. Mastorakos, Ignition of turbulent non-premixed flames, Prog. Energy Combust. Sci. 35 (1) (2009) 57–97.
[29] S.P.M. Bane, Spark Ignition: Experimental and Numerical Investigation with Application to Aviation Safety (Ph.D. thesis), California Institute of Technology, 2010.
[30] D. Bradley, C. Sheppard, I. Suardjaja, R. Woolley, Fundamentals of high-energy spark ignition with lasers, Combust. Flame 138 (1–2) (2004) 55–77.
[31] Y. Ju, W. Sun, Plasma assisted combustion: Dynamics and chemistry, Prog. Energy Combust. Sci. 48 (2015) 21–83.
[32] E. Mastorakos, Forced ignition of turbulent spray flames, Proc. Combust. Inst. 36 (2) (2017) 2367–2383.
[33] S.S. Shy, Spark ignition transitions in premixed turbulent combustion, Prog. Energy Combust. Sci. 98 (2023) 101099.
[34] D. Yu, Z. Chen, Premixed flame ignition: Theoretical development, Prog. Energy Combust. Sci. 104 (2024) 101174.
[35] R.W. Read, Experimental investigations into high-altitude relight of a gas turbine (Ph.D. thesis), University of Cambridge, 2008.
[36] S. Tsuboi, S. Miyokawa, M. Matsuda, T. Yokomori, N. Iida, Influence of spark discharge characteristics on ignition and combustion process and the lean operation limit in a spark ignition engine, Appl. Energy 250 (2019) 617–632.
[37] Y. Ban, F. Zhang, Z. Zhang, Z. Li, X. Qi, Y. Tian, J. Zhu, Y. Pei, S. Zhong, A comparative numerical study of plasma and spark assisted ignition in a cavity-based supersonic combustor, Combust. Flame 284 (2026) 114620.
[38] D. Yu, Z. Chen, Theoretical analysis on the transient ignition of a premixed expanding flame in a quiescent mixture, J. Fluid Mech. 924 (2021) A22.
[39] D. Yu, X. Chen, Z. Chen, Analysis on ignition kernel formation in a quiescent mixture: different characteristic time scales and critical heating powers, Combust. Flame 245 (2022) 112336.
[40] M. Champion, B. Deshaies, G. Joulin, Relative influences of convective and diffusive transports during spherical flame initiation, Combust. Flame 74 (2) (1988) 161–170.
[41] L. He, Critical conditions for spherical flame initiation in mixtures with high Lewis numbers, Combust. Theory Model. 4 (2) (2000) 159–172.
[42] Z. Chen, Y. Ju, Theoretical analysis of the evolution from ignition kernel to flame ball and planar flame, Combust. Theory Model. 11 (3) (2007) 427–453.
[43] Z. Chen, M.P. Burke, Y. Ju, On the critical flame radius and minimum ignition energy for spherical flame initiation, Proc. Combust. Inst. 33 (1) (2011) 1219–1226.
[44] Y. Ju, C.B. Reuter, O.R. Yehia, T.I. Farouk, S.H. Won, Dynamics of cool flames, Prog. Energy Combust. Sci. 75 (2019) 100787.
[45] Y. Ju, Understanding cool flames and warm flames, Proc. Combust. Inst. 38 (1) (2021) 83–119.
[46] F. Wu, A. Saha, S. Chaudhuri, C.K. Law, Facilitated ignition in turbulence through differential diffusion, Phys. Rev. Lett. 113 (2) (2014) 024503.
[47] S.S. Shy, M.T. Nguyen, S.Y. Huang, Effects of electrode spark gap, differential diffusion, and turbulent dissipation on two distinct phenomena: turbulent facilitated ignition versus minimum ignition energy transition, Combust. Flame 205 (2019) 371–377.
[48] H.A. Uranakara, S. Chaudhuri, K.N. Lakshmisha, On the extinction of igniting kernels in near-isotropic turbulence, Proc. Combust. Inst. 36 (2) (2017) 1793–1800.
[49] P. Clavin, Dynamic behavior of premixed flame fronts in laminar and turbulent flows, Prog. Energy Combust. Sci. 11 (1) (1985) 1–59.
[50] P. Clavin, Dynamics of combustion fronts in premixed gases: from flames to detonations, Proc. Combust. Inst. 28 (1) (2000) 569–585.
[51] C.K. Law, C.J. Sung, Structure, aerodynamics, and geometry of premixed flamelets, Prog. Energy Combust. Sci. 26 (4–6) (2000) 459–505.
[52] J. Buckmaster, P. Clavin, A. Liñan, M. Matalon, N. Peters, G. Sivashinsky, F.A. Williams, Combustion theory and modeling, Proc. Combust. Inst. 30 (1) (2005) 1–19.
[53] M. Matalon, Flame dynamics, Proc. Combust. Inst. 32 (1) (2009) 57–82.
[54] L.P.H. de Goey, J.A. van Oijen, V.N. Kornilov, J.H.M. ten Thije Boonkkamp, Propagation, dynamics and control of laminar premixed flames, Proc. Combust. Inst. 33 (1) (2011) 863–886.
[55] H. Pitsch, The transition to sustainable combustion: Hydrogen- and carbon-based future fuels and methods for dealing with their challenges, Proc. Combust. Inst. 40 (2024) 105638.
[56] J.B. Heywood, Internal Combustion Engine Fundamentals, second ed., McGraw-Hill Education, 2018.
[57] Z. Wang, H. Liu, R.D. Reitz, Knocking combustion in spark-ignition engines, Prog. Energy Combust. Sci. 61 (2017) 78–112.
[58] L. Zhou, X. Zhang, K.H. Luo, H. Wei, End-gas autoignition and detonation in confined space, Prog. Energy Combust. Sci. 108 (2025) 101217.

[59] F. Egolfopoulos, N. Hansen, Y. Ju, K. Kohse-Höinghaus, C. Law, F. Qi, Advances and challenges in laminar flame experiments and implications for combustion chemistry, Prog. Energy Combust. Sci. 43 (2014) 36–67.

[60] Z. Chen, On the accuracy of laminar flame speeds measured from outwardly propagating spherical flames: Methane/air at normal temperature and pressure, Combust. Flame 162 (6) (2015) 2442–2453.

[61] M. Faghih, Z. Chen, The constant-volume propagating spherical flame method for laminar flame speed measurement, Sci. Bull. 61 (16) (2016) 1296–1310.

[62] A.A. Konnov, A. Mohammad, V.R. Kishore, N.I. Kim, C. Prathap, S. Kumar, A comprehensive review of measurements and data analysis of laminar burning velocities for various fuel+air mixtures, Prog. Energy Combust. Sci. 68 (2018) 197–267.

[63] S. Hochgreb, How fast can we burn, 2.0, Proc. Combust. Inst. 39 (2) (2023) 2077–2105.

[64] C. Xiouris, T. Ye, J. Jayachandran, F.N. Egolfopoulos, Laminar flame speeds under engine-relevant conditions: Uncertainty quantification and minimization in spherically expanding flame experiments, Combust. Flame 163 (2016) 270–283.

[65] A. Movaghar, R. Lawson, F.N. Egolfopoulos, Confined spherically expanding flame method for measuring laminar flame speeds: Revisiting the assumptions and application to C1–C4 hydrocarbon flames, Combust. Flame 212 (2020) 79–92.

[66] R. Lawson, V. Gururajan, A. Movaghar, F.N. Egolfopoulos, Autoignition of reacting mixtures at engine-relevant conditions using confined spherically expanding flames, Proc. Combust. Inst. 38 (2) (2021) 2285–2293.

[67] K. Van, A. Hu, M. Rubio, J.Z. Fang, B. Sarkar, T.K. Bera, A.A. Aradi, F.N. Egolfopoulos, Effects of end-gas reactivity on fundamental combustion properties of primary reference fuel blends with ethanol at engine-relevant conditions, Combust. Flame 282 (2025) 114524.

[68] K. Van, A. Hu, J.Z. Fang, T.K. Bera, A.A. Aradi, S.K. Jain, F.N. Egolfopoulos, Quantitative studies of instabilities of confined spherically expanding flames: Application to flame propagation and autoignition of natural gas blends with hydrogen at engine-relevant conditions, Combust. Flame 274 (2025) 114009.

[69] A. Hu, K. Van, S. Oh, J.-W. Park, Y. Pei, F.N. Egolfopoulos, Propagation of laminar hydrogen flames at high pressures and temperatures, Combust. Flame 288 (2026) 114953.

[70] A.M. Ferris, A.J. Susa, D.F. Davidson, R.K. Hanson, High-temperature laminar flame speed measurements in a shock tube, Combust. Flame 205 (2019) 241–252.

[71] A.J. Susa, A.M. Ferris, D.F. Davidson, R.K. Hanson, Experimental study of autoignition and double flame structure in shock tube, AIAA J. 57 (10) (2019) 4476–4481.

[72] A.J. Susa, A.M. Ferris, D.F. Davidson, R.K. Hanson, Experimental shock tube measurements of laminar burning velocity of n-heptane and iso-octane in the negative temperature coefficient regime, in: AIAA-2019-0460, 2019.

[73] A.J. Susa, D.F. Davidson, R.K. Hanson, Gravity-current-induced test gas stratification and its prevention in constrained reaction volume shock-tube experiments, Shock Waves 29 (2019) 1091–1098.

[74] A.J. Susa, R.K. Hanson, Simultaneous side-wall-schlieren and -emission imaging of autoignition phenomena in conventional and constrained-reaction-volume shock-tube experiments, Proc. Combust. Inst. 39 (1) (2023) 1377–1386.

[75] A.J. Susa, L. Zheng, R.K. Hanson, Measurements of propane–O_2–ar laminar flame speeds at temperatures exceeding 1000 k in a shock tube, Proc. Combust. Inst. 39 (2) (2023) 1793–1802.

[76] L. Zheng, M. Figueroa-Labastida, J.W. Streicher, A.M. Ferris, R.K. Hanson, Experimental measurements of n-heptane flame speeds behind reflected shock waves with variable extents of pre-flame auto-ignition chemistry, Combust. Flame 261 (2024) 113290.

[77] L. Zheng, M. Figueroa-Labastida, C. Wei, R.K. Hanson, Effect of pre-flame reaction extent on the dynamics of outwardly expanding dimethyl ether (DME) laminar flames in the NTC region, Combust. Flame 276 (2026) 115001.

[78] D. Assanis, S.W. Wagnon, M.S. Wooldridge, An experimental study of flame and autoignition interactions of iso-octane and air mixtures, Combust. Flame 162 (4) (2015) 1214–1224.

[79] Q. Fan, Y. Qi, Y. Wang, Z. Wang, Investigation into pressure dependence of flame speed for fuels with low and high octane sensitivity through blending ethanol, Combust. Flame 212 (2020) 252–269.

[80] J. Klein, O. Samimi-Abianeh, Laminar flame speed regime at elevated temperature and pressure, Fuel 368 (2024) 131672.

[81] A. Gambardella, V. De Bellis, J. Hyvonen, E. Malfi, Laminar flame speed of methane–air mixtures under engine-relevant thermodynamic conditions: RCEM measurements and correlation development, Fuel 427 (2027) 139784.

[82] Y.B. Zel'dovich, V. Librovich, G. Makhviladze, G. Sivashinsky, On the development of detonation in a non-uniformly preheated gas, Astronaut. Acta 15 (5–6) (1970) 313–321.

[83] Y.B. Zeldovich, Regime classification of an exothermic reaction with nonuniform initial conditions, Combust. Flame 39 (2) (1980) 211–214.

[84] D. Bradley, C. Morley, X. Gu, D. Emerson, Amplified pressure waves during autoignition: relevance to CAI engines, in: SAE-2002-01-2868, 2002.

[85] X. Gu, D. Emerson, D. Bradley, Modes of reaction front propagation from hot spots, Combust. Flame 133 (1–2) (2003) 63–74.

[86] M.-B. Sun, X.-D. Cui, H.-B. Wang, V. Bychkov, Flame flashback in a supersonic combustor fueled by ethylene with cavity flameholder, J. Propuls. Power 31 (3) (2015) 976–981.

[87] Z.-G. Wang, M.-B. Sun, H.-B. Wang, J.-F. Yu, J.-H. Liang, F.-C. Zhuang, Mixing-related low frequency oscillation of combustion in an ethylene-fueled supersonic combustor, Proc. Combust. Inst. 35 (2) (2015) 2137–2144.

[88] P. Ronney, Understanding combustion processes through microgravity research, Proc. Combust. Inst. 27 (1998) 2485–2506.

[89] P. Clavin, Quasi-isobaric ignition near the flammability limits. Flame balls and self-extinguishing flames, Combust. Flame 179 (2017) 80–90.

[90] Y.B. Zeldovich, G.I. Barenblatt, V. Librovich, G. Makhviladze, The Mathematical Theory of Combustion and Explosions, Consultants Bureau, New York, 1985.

[91] B. Lewis, G. Von Elbe, Combustion, Flames and Explosions of Gases, third ed., Elsevier, New York, 2012.

[92] D. Yu, Z. Chen, Theoretical analysis on the forced ignition of a quiescent mixture by repetitive heating pulse, Proc. Combust. Inst. 39 (2) (2023) 1881–1891.

[93] D. Yu, L. Yue, Z. Chen, Theoretical analysis on the forced ignition of a quiescent mixture by heat and radical sources, Proc. Combust. Inst. 40 (2024) 105549.

[94] J.W. Dold, Premixed flames modelled with thermally sensitive intermediate branching kinetics, Combust. Theory Model. 11 (6) (2007) 909–948.

[95] H. Zhang, Z. Chen, Spherical flame initiation and propagation with thermally sensitive intermediate kinetics, Combust. Flame 158 (8) (2011) 1520–1531.

[96] H. Zhang, P. Guo, Z. Chen, Critical condition for the ignition of reactant mixture by radical deposition, Proc. Combust. Inst. 34 (2) (2013) 3267–3275.

[97] W. Han, Z. Chen, Effects of finite-rate droplet evaporation on the ignition and propagation of premixed spherical spray flame, Combust. Flame 162 (5) (2015) 2128–2139.

[98] S.P.M. Bane, J.L. Ziegler, P.A. Boettcher, S.A. Coronel, J.E. Shepherd, Experimental investigation of spark ignition energy in kerosene, hexane, and hydrogen, J. Loss Prev. Process. Ind. 26 (2011) 290–294.

[99] W. Zhang, M. Faqih, X. Gou, Z. Chen, Numerical study on the transient evolution of a premixed cool flame, Combust. Flame 187 (2018) 129–136.

[100] Q. Yang, P. Zhao, Minimum ignition energy and propagation dynamics of laminar premixed cool flames, Proc. Combust. Inst. 38 (2) (2021) 2315–2322.

[101] Y. Wang, S. Xie, H. Böttler, Y. Wang, X. Chen, A. Scholtissek, C. Hasse, Z. Chen, Forced ignition of premixed cool and hot DME/air flames in a laminar counterflow, Combust. Flame 259 (2024) 113169.

[102] L. Benteux, X. Hu, W. Liang, C.K. Law, D.M. Valiev, Steady hot and cool dimethyl ether premixed flames in channels with wall heat loss, Combust. Flame 274 (2025) 113982.

[103] Y. Wang, W. Han, T. Zirwes, F. Zhang, H. Bockhorn, Z. Chen, Effects of low-temperature chemical reactions on ignition kernel development and flame propagation in a DME-air mixing layer, Proc. Combust. Inst. 39 (2) (2023) 1515–1524.

[104] Y. Wang, Y. Wang, X. Chen, S. Xie, H. Böttler, A. Scholtissek, C. Hasse, Z. Chen, Forced ignition of cool, warm and hot flames in a laminar non-premixed counterflow of DME versus air, Proc. Combust. Inst. 40 (1–4) (2024) 105222.

[105] S. Xie, X. Chen, Y. Wang, T. Zhang, Z. Chen, Numerical study on forced ignition and flame propagation in a counterflow of nitrogen-diluted hydrogen versus air, Fuel 357 (2024) 129863.

[106] D.R. Ballal, A.H. Lefebvre, The influence of spark discharge characteristics on minimum ignition energy in flowing gases, Combust. Flame 24 (1975) 99–108.

[107] J.-L. Beduneau, B. Kim, L. Zimmer, Y. Ikeda, Measurements of minimum ignition energy in premixed laminar methane/air flow by using laser induced spark, Combust. Flame 132 (4) (2003) 653–665.

[108] Y. Kobayashi, S. Nakaya, M. Tsue, Laser-induced spark ignition for DME-air mixtures with low velocity, Proc. Combust. Inst. 37 (4) (2019) 4127–4135.

[109] V.R. Katta, J.M. Bonebrake, D.L. Blunck, T.M. Ombrello, Propagation of ignition kernel in CO_2-diluted, CH_4/air mixtures, Combust. Flame 229 (2021) 111380.

[110] S. Jo, J.P. Gore, Laser ignition energy for turbulent premixed hydrogen air jets, Combust. Flame 236 (2022) 111767.

[111] X. Mao, H. Zhong, Z. Wang, T. Ombrello, Y. Ju, Effects of inter-pulse coupling on nanosecond pulsed high frequency discharge ignition in a flowing mixture, Proc. Combust. Inst. 39 (4) (2023) 5457–5464.

[112] J.K. Lefkowitz, T. Ombrello, An exploration of inter-pulse coupling in nanosecond pulsed high frequency discharge ignition, Combust. Flame 180 (2017) 136–147.

[113] J.K. Lefkowitz, T. Ombrello, Reduction of flame development time in nanosecond pulsed high frequency discharge ignition of flowing mixtures, Combust. Flame 193 (2018) 471–480.

[114] S. Shen, I. Laso, N. Rozin, J.K. Lefkowitz, On pulse energy and energy distribution for ignition of flowing mixtures, Proc. Combust. Inst. 39 (2023) 5487–5498.

[115] S. Shen, E. Rempe, W. Senior-Tybora, J.K. Lefkowitz, Destructive inter-pulse coupling in nanosecond-pulsed high-frequency discharge ignition: Effect of hydrodynamic regimes, Proc. Combust. Inst. 40 (2024) 105445.

[116] T.S. Taneja, T. Ombrello, J. Lefkowitz, S. Yang, Large eddy simulation of plasma assisted ignition: Effects of pulse repetition frequency, number of pulses, and pulse energy, Combust. Flame 267 (2024) 113574.

[117] S.S. Shy, Y.C. Liao, Y.R. Chen, S.Y. Huang, Two ignition transition modes at small and large distances between electrodes of a lean primary reference automobile fuel/air mixture at 373 k with Lewis number ≫ 1, Combust. Flame 225 (2021) 340–348.

[118] X. Chen, S. Xie, H. Böttler, A. Scholtissek, W. Han, D. Yu, C. Hasse, Z. Chen, Effects of electrodes and imposed flow on forced ignition in laminar premixed hydrogen/air mixtures with large Lewis number, Proc. Combust. Inst. 39 (2) (2023) 1967–1976.

[119] X. Chen, H. Böttler, S. Xie, A. Scholtissek, W. Han, C. Hasse, Z. Chen, On the flow-facilitated ignition in a mixture with low Lewis number, Combust. Flame 258 (2023) 113091.

[120] V.T. Mai, S.S. Shy, An experimental investigation on a flow-facilitated ignition at reduced and normal pressures for small, near-unity and large Lewis number of hydrogen/air and hydrogen/ammonia/air mixtures, Combust. Flame 270 (2024) 113746.

[121] P.A. Boettcher, Thermal Ignition (Ph.D. thesis), California Institute of Technology, 2012.

[122] P.A. Boettcher, S.K. Menon, B.L. Ventura, G. Blanquart, J.E. Shepherd, Cyclic flame propagation in premixed combustion, J. Fluid Mech. 735 (2013) 176–202.

[123] S.K. Menon, P.A. Boettcher, B. Ventura, G. Blanquart, Hot surface ignition of n-hexane in air, Combust. Flame 163 (2016) 42–53.

[124] L.R. Boeck, M. Meijers, A. Kink, R. Mével, J.E. Shepherd, Ignition of fuel-air mixtures from a hot circular cylinder, Combust. Flame 185 (2017) 265–277.

[125] L.R. Boeck, J. Melguizo-Gavilanes, J.E. Shepherd, Hot surface ignition dynamics in premixed hydrogen-air near the lean flammability limit, Combust. Flame 210 (2019) 467–478.

[126] S. Jones, J. Shepherd, Thermal ignition by vertical cylinders, Combust. Flame 232 (2021) 111499.

[127] J.L. Urban, Spot Ignition of Natural Fuels by Hot Metal Particles (Ph.D. thesis), University of California, Berkeley, 2017.

[128] S.A. Coronel, Thermal Ignition Using Moving Hot Particles (Ph.D. thesis), California Institute of Technology, 2016.

[129] D. Roth, P. Sharma, T. Haeber, R. Schiessl, H. Bockhorn, U. Maas, Ignition by mechanical sparks: ignition of hydrogen/air mixtures by submillimeter-sized hot particles, Combust. Sci. Technol. 186 (10–11) (2014) 1606–1617.

[130] D. Roth, T. Haber, H. Bockhorn, Experimental and numerical study on the ignition of fuel/air mixtures at laser heated silicon nitride particles, Proc. Combust. Inst. 36 (1) (2017) 1475–1484.

[131] T. Haber, T. Zirwes, D. Roth, F. Zhang, H. Bockhorn, U. Maas, Numerical simulation of the ignition of fuel/air gas mixtures around small hot particles, Z. Phys. Chem. 231 (2017) 1625–1654.

[132] J. Melguizo-Gavilanes, R. Mével, S. Coronel, J.E. Shepherd, Effects of differential diffusion on ignition of stoichiometric hydrogen-air by moving hot spheres, Proc. Combust. Inst. 36 (1) (2017) 1155–1163.

[133] S.A. Coronel, J. Melguizo-Gavilanes, R. Mével, J.E. Shepherd, Experimental and numerical study on moving hot particle ignition, Combust. Flame 192 (2018) 495–506.

[134] T. Zirwes, F. Zhang, T. Haber, H. Bockhorn, Ignition of combustible mixtures by hot particles at varying relative speeds, Combust. Sci. Technol. 191 (1) (2019) 178–195.

[135] S. Jones, J. Melguizo-Gavilanes, J.E. Shepherd, Ignition by moving hot spheres in H_2-O_2-N_2 environments, Proc. Combust. Inst. 37 (1) (2019) 1597–1604.

[136] Y. Wang, H. Zhang, T. Zirwes, F. Zhang, H. Bockhorn, Z. Chen, Ignition of dimethyl ether/air mixtures by hot particles: Impact of low temperature chemical reactions, Proc. Combust. Inst. 38 (2) (2021) 2459–2466.

[137] D. Yu, Z. Chen, Theoretical analysis on the ignition of a combustible mixture by a hot particle, J. Fluid Mech. 936 (2022) A22.

[138] Y. Wang, S. Li, Y. Wang, D. Yu, H. Zhang, Z. Chen, Analysis of the ignition of hydrogen/air mixtures induced by a hot particle, Phys. Chem. Chem. Phys. 24 (2022) 21188.

[139] Y. Wang, Z. Chen, Effects of Particle Size on the Ignition of Static CH_4/Air and H_2/Air Mixtures by Hot Particles, Combust. Sci. Technol. 194 (5) (2022) 869–881.

[140] Y. Morii, K. Maruta, General concept for autoignitive reaction wave covering from subsonic to supersonic regimes, Phys. Fluids 36 (1) (2024) 016139.

[141] A. Cavaliere, M. de Joannon, Mild combustion, Prog. Energy Combust. Sci. 30 (4) (2004) 329–366.

[142] P. Li, J. Mi, B.B. Dally, F. Wang, L. Wang, Z. Liu, S. Chen, C. Zheng, Progress and recent trend in MILD combustion, Sci. China Technol. Sci. 54 (2) (2011) 255–269.

[143] B.C. Choi, K.N. Kim, S.H. Chung, Autoignited laminar lifted flames of propane in coflow jets with tribrachial edge and mild combustion, Combust. Flame 156 (2) (2009) 396–404.

[144] K.S. Jung, B.R. Jung, S.H. Kang, S.H. Chung, C.S. Yoo, A numerical study of the pyrolysis effect on autoignited laminar lifted dimethyl ether jet flames in heated coflow air, Combust. Flame 209 (2019) 1–13.

[145] J.C. Livengood, P.C. Wu, Correlation of autoignition phenomena in internal combustion engines and rapid compression machines, Proc. Combust. Inst. 5 (1955) 347–356.

[146] J. Pan, P. Zhao, C.K. Law, H. Wei, A predictive Livengood–Wu correlation for two-stage ignition, Int. J. Engine Res. 17 (8) (2016) 825–835.

[147] X. Chen, P. Zhao, P. Dai, Z. Chen, On the prediction of hot spot induced ignition by the Livengood-Wu integral, Proc. Combust. Inst. 38 (3) (2021) 4709–4716.

[148] L. Kagan, G. Sivashinsky, Hydrodynamic aspects of end-gas autoignition, Proc. Combust. Inst. 34 (1) (2013) 857–863.

[149] L. Yang, Y. Wang, Z. Chen, Comparison of combustion duration and end-gas autoignition in inwardly and outwardly propagating flames induced by different ignition configurations, Combust. Theory Model. 27 (1) (2023) 103–117.

[150] Y. Ju, W. Sun, M.P. Burke, X. Gou, Z. Chen, Numerical study of spark-assisted flame propagation in n-heptane/air mixtures, Proc. Combust. Inst. 33 (1) (2011) 1245–1251.

[151] J.B. Martz, G.A. Lavoie, H.G. Im, R.J. Middleton, A. Babajimopoulos, D.N. Assanis, The propagation of a laminar reaction front during end-gas auto-ignition, Combust. Flame 159 (6) (2012) 2077–2086.

[152] H. Yu, Z. Chen, End-gas autoignition and detonation development in a closed chamber, Combust. Flame 162 (11) (2015) 4102–4111.

[153] H. Terashima, M. Koshi, Mechanisms of strong pressure wave generation in end-gas autoignition during knocking combustion, Combust. Flame 162 (5) (2015) 1944–1956.

[154] J. Pan, G. Shu, P. Zhao, H. Wei, Z. Chen, Interactions of flame propagation, auto-ignition and pressure wave during knocking combustion, Combust. Flame 164 (2016) 319–328.

[155] J. Pan, H. Wei, G. Shu, Z. Chen, P. Zhao, The role of low temperature chemistry in combustion mode development under elevated pressures, Combust. Flame 174 (2016) 179–193.

[156] H. Yu, C. Qi, Z. Chen, Effects of flame propagation speed and chamber size on end-gas autoignition, Proc. Combust. Inst. 36 (3) (2017) 3533–3541.

[157] H. Terashima, A. Matsugi, M. Koshi, Origin and reactivity of hot-spots in end-gas autoignition with effects of negative temperature coefficients: Relevance to pressure wave developments, Combust. Flame 184 (2017) 324–334.

[158] H. Terashima, A. Matsugi, M. Koshi, End-gas autoignition behaviors under pressure wave disturbance, Combust. Flame 203 (2019) 204–216.

[159] A. Robert, S. Richard, O. Colin, L. Martinez, L.D. Franqueville, LES prediction and analysis of knocking combustion in a spark ignition engine, Proc. Combust. Inst. 35 (3) (2015) 2941–2948.

[160] Y. Morii, A.K. Dubey, H. Nakamura, K. Maruta, Two-dimensional laboratory-scale DNS for knocking experiment using n-heptane at engine-like condition, Combust. Flame 223 (2021) 330–336.

[161] H.A. El-Asrag, Y. Ju, Direct numerical simulations of NO_x effect on multistage autoignition of DME/air mixture in the negative temperature coefficient regime for stratified HCCI engine conditions, Combust. Flame 161 (1) (2014) 256–269.

[162] A. Krisman, E.R. Hawkes, M. Talei, A. Bhagatwala, J.H. Chen, A direct numerical simulation of cool-flame affected autoignition in diesel engine-relevant conditions, Proc. Combust. Inst. 36 (3) (2017) 3567–3575.

[163] H. Wei, C. Chen, H. Zhou, W. Zhao, Z. Ren, Effect of turbulent mixing on the end gas auto-ignition of n-heptane/air mixtures under IC engine-relevant conditions, Combust. Flame 174 (2016) 25–36.

[164] H. Wei, J. Zhao, L. Zhou, D. Gao, Z. Xu, Effects of the equivalence ratio on turbulent flame–shock interactions in a confined space, Combust. Flame 186 (2017) 247–262.

[165] J. Urzay, Supersonic combustion in air-breathing propulsion systems for hypersonic flight, Annu. Rev. Fluid Mech. 50 (2018) 593–627.

[166] Z. Cai, T. Wang, M. Sun, Review of cavity ignition in supersonic flows, Acta Astronaut. 165 (2019) 268–286.

[167] F. Kaufmann, P. Roth, Numerical simulation of one-dimensional laminar flames propagating into reacting premixed gases, Combust. Flame 81 (1990) 300–307.

[168] P. Habisreuther, F.C.C. Galeazzo, C. Prathap, N. Zarzalis, Structure of laminar premixed flames of methane near the auto-ignition limit, Combust. Flame 160 (12) (2013) 2770–2782.

[169] J.B. Martz, H. Kwak, H.G. Im, G.A. Lavoie, D.N. Assanis, Propagation of a reacting front in an auto-igniting mixture, in: 6th US National Combustion Meeting, Ann Arbor, Michigan, 2009.

[170] J.B. Martz, H. Kwak, H.G. Im, G.A. Lavoie, D.N. Assanis, Combustion regime of a reacting front propagating into an auto-igniting mixture, Proc. Combust. Inst. 33 (2) (2011) 3001–3006.

[171] J. Pan, G. Shu, H. Wei, M. Pan, A NTC-affected reaction front propagating into autoigniting mixtures, in: 10th Asia-Pacific Conference on Combustion, ASPACC, Beijing, China, 2015.

[172] J. Pan, G. Shu, H. Wei, M. Pan, Hydrogen addition effect on a reaction front propagation in NTC-affected auto-igniting mixture, Int. J. Hydrog. Energy 40 (26) (2015) 8083–8093.

[173] R. Sankaran, Propagation velocity of a deflagration front in a preheated autoigniting mixture, in: 9th US National Combustion Meeting, Central States Section of the Combustion Institute, Cincinnati, Ohio, 2015.

[174] A. Krisman, E.R. Hawkes, J.H. Chen, The structure and propagation of laminar flames under autoignitive conditions, Combust. Flame 188 (2018) 399–411.

[175] A. Krisman, C. Mounaim-Rousselle, R. Sivaramakrishnan, J.A. Miller, J.H. Chen, Reference natural gas flames at nominally autoignitive engine-relevant conditions, Proc. Combust. Inst. 37 (2) (2019) 1631–1638.
[176] Q. Yang, Z. Chen, A.J. Susa, R.K. Hanson, P. Zhao, Thermal-pyrolysis induced over-driven flame and its potential role in the negative-temperature dependence of iso-octane flame speed at elevated temperatures, Combust. Flame 225 (2021) 344–352.
[177] T. Zhang, A.J. Susa, R.K. Hanson, Y. Ju, Studies of the dynamics of autoignition-assisted outwardly propagating spherical cool and double flames under shock-tube conditions, Proc. Combust. Inst. 38 (2) (2021) 2275–2283.
[178] T. Goyal, O. Samimi-Abianeh, Measurement and simulation of autoignition-assisted flame speed of N-heptane mixture at elevated gas temperature, Ind. Eng. Chem. Res. 62 (17) (2023) 6737–6749.
[179] T. Goyal, M. Klein, O. Samimi-Abianeh, Numerical and experimental study of autoignition-assisted premixed n-heptane flames using RCM-flame apparatus, Combust. Flame 258 (2023) 113074.
[180] Y. Wang, A. Movaghar, Z. Wang, Z. Liu, W. Sun, F.N. Egolfopoulos, Z. Chen, Laminar flame speeds of methane/air mixtures at engine conditions: Performance of different kinetic models and power-law correlations, Combust. Flame 218 (2020) 101–108.
[181] M. Faghih, H. Li, X. Gou, Z. Chen, On laminar premixed flame propagating into autoigniting mixtures under engine-relevant conditions, Proc. Combust. Inst. 37 (4) (2019) 4673–4680.
[182] T. Zhang, Y. Ju, Structures and propagation speeds of autoignition-assisted premixed n-heptane/air cool and warm flames at elevated temperatures and pressures, Combust. Flame 211 (2020) 8–17.
[183] X. Gong, Z. Ren, Flame speed scaling in autoignition-assisted freely propagating n-heptane/air flames, Proc. Combust. Inst. 38 (2) (2021) 2153–2161.
[184] X. Gong, Q. Xie, H. Zhou, Z. Ren, Structure and propagation speed of autoignition-assisted flames of jet fuels, Combust. Flame 237 (2022) 111810.
[185] A. Ansari, J. Jayachandran, F.N. Egolfopoulos, Parameters influencing the burning rate of laminar flames propagating into a reacting mixture, Proc. Combust. Inst. 37 (2) (2019) 1707–1714.
[186] S. Desai, R. Sankaran, H.G. Im, Unsteady deflagration speed of an auto-ignitive dimethyl-ether (DME)/air mixture at stratified conditions, Proc. Combust. Inst. 37 (2) (2019) 4717–4725.
[187] B.S. Soriano, E.S. Richardson, Investigation of flame propagation in autoignitive blends of n-heptane and methane fuel, Combust. Theory Model. 23 (6) (2019) 1054–1070.
[188] H. Lin, P. Zhao, H. Ge, A computational study on laminar flame propagation in mixtures with non-zero reaction progress, in: SAE-2019-01-0946, 2019.
[189] G. Xiao, H. Ge, P. Zhao, Initiation and propagation of one-dimensional planar flames in mixtures with variable reaction progress, Combust. Flame 236 (2022) 111765.
[190] K. Akita, P. Zhao, Y. Morii, K. Maruta, D. Splitter, F. Dal Forno Chuahy, Effects of unburnt reaction progress on stretch flame dynamics under elevated temperatures, Combust. Flame 261 (2024) 113316.
[191] H. Tajima, T. Tomidokoro, T. Yokomori, Effects of reaction progress on the laminar flame speed of gasoline/air mixtures under engine-relevant conditions, Proc. Combust. Inst. 40 (2024) 105734.
[192] A. Tsunoda, Y. Morii, K. Maruta, Theoretical framework for knock onset: ZFK–FKPP-transition-based analysis of flame acceleration with a chemically unfrozen preheat zone, Combust. Flame 291 (2026) 115121.
[193] D.J. Micka, J.F. Driscoll, Stratified jet flames in a heated (1390 k) air cross-flow with autoignition, Combust. Flame 159 (4) (2012) 1205–1214.
[194] J.F. Driscoll, J.H. Chen, A.W. Skiba, C.D. Carter, E.R. Hawkes, H. Wang, Premixed flames subjected to extreme turbulence: Some questions and recent answers, Prog. Energy Combust. Sci. 76 (2020) 100802.
[195] H. Pers, A. Aniello, F. Morisseau, T. Schuller, Autoignition-induced flashback in hydrogen-enriched laminar premixed burners, Int. J. Hydrog. Energy 48 (27) (2023) 10235–10249.
[196] B. Savard, E.R. Hawkes, K. Aditya, H. Wang, J.H. Chen, Regimes of premixed turbulent spontaneous ignition and deflagration under gas-turbine reheat combustion conditions, Combust. Flame 208 (2019) 402–419.
[197] S. Farjam, B. Savard, Ignition and flame stabilization of n-dodecane turbulent premixed flames under Spray A thermochemical conditions, Combust. Flame 242 (2022) 112133.
[198] K. Aditya, A. Gruber, C. Xu, T. Lu, A. Krisman, M.R. Bothien, J.H. Chen, Direct numerical simulation of flame stabilization assisted by autoignition in a reheat gas turbine combustor, Proc. Combust. Inst. 37 (2) (2019) 2635–2642.
[199] A. Gruber, M.R. Bothien, A. Ciani, K. Aditya, J.H. Chen, F.A. Williams, Direct numerical simulation of hydrogen combustion at auto-ignitive conditions: Ignition, stability and turbulent reaction-front velocity, Combust. Flame 224 (2021) 32–50.
[200] T. Lu, C.S. Yoo, J.H. Chen, C.K. Law, Three-dimensional direct numerical simulation of a turbulent lifted hydrogen jet flame in heated coflow: a chemical explosive mode analysis, J. Fluid Mech. 652 (2010) 45–64.
[201] R. Shan, C.S. Yoo, J.H. Chen, T. Lu, Computational diagnostics for n-heptane flames with chemical explosive mode analysis, Combust. Flame 159 (10) (2012) 3119–3127.
[202] C. Xu, J.-W. Park, C.S. Yoo, J.H. Chen, T. Lu, Identification of premixed flame propagation modes using chemical explosive mode analysis, Proc. Combust. Inst. 37 (2) (2019) 2407–2415.
[203] W. Wu, Y. Piao, Q. Xie, Z. Ren, Flame diagnostics with a conservative representation of chemical explosive mode analysis, AIAA J. 57 (4) (2019) 1355–1363.
[204] S. Goldsborough, S. Hochgreb, G. Vanhove, M. Wooldridge, H. Curran, C.-J. Sung, Advances in rapid compression machine studies of low- and intermediate-temperature autoignition phenomena, Prog. Energy Combust. Sci. 63 (2017) 1–78.
[205] A.B. Mansfield, M.S. Wooldridge, High-pressure low-temperature ignition behavior of syngas mixtures, Combust. Flame 161 (2014) 2242–2251.
[206] H. Im, P. Pal, M. Wooldridge, A. Mansfield, A regime diagram for autoignition of homogeneous reactant mixtures with turbulent velocity and temperature fluctuations, Combust. Sci. Technol. 187 (8) (2015) 1263–1275.
[207] K.P. Grogan, S.S. Goldsborough, M. Ihme, Ignition regimes in rapid compression machines, Combust. Flame 162 (2015) 3071–3080.
[208] M.A. Burnett, M.S. Wooldridge, An experimental investigation of flame and autoignition behavior of propane, Combust. Flame 224 (2021) 24–32.
[209] M. Figueroa-Labastida, M.B. Luong, J. Badra, H.G. Im, A. Farooq, Experimental and computational studies of methanol and ethanol preignition behind reflected shock waves, Combust. Flame 234 (2021) 111621.
[210] A.D. Kiverin, K.O. Minaev, I.S. Yakovenko, Modes of mild ignition in shock tubes: Origins and classification, Combust. Flame 221 (2020) 420–428.
[211] C. Huang, Y. Wang, R. Deiterding, D. Yu, Z. Chen, Numerical study on weak and strong ignition induced by reflected shock and boundary layer interaction, Acta Mech. Sin. 38 (2022) 121466.
[212] Y. Wang, X. Guan, S. Xie, M. Zhou, Z. Zhang, Z. Chen, T. Zhang, Numerical studies on the ignition and propagation for spherically expanding premixed cool flames under gravitational conditions, Combust. Flame 268 (2024) 113577.
[213] B. Savard, A. Wehrfritz, K. Lam, Q. Margerte, L. Ferney, S. Farjam, Decreased mixture reactivity and hot flame speed in the products of diffusion-affected autoignitive cool flames in the NTC regime, Combust. Flame 222 (2020) 434–445.
[214] Y. Wang, W. Han, Z. Chen, Effects of stratification on premixed cool flame propagation and modeling, Combust. Flame 229 (2021) 111394.
[215] X. Shi, J.-Y. Chen, Numerical analysis and model development for laminar flame speed of stratified methane/air mixtures, Combust. Flame 184 (2017) 233–245.
[216] G. Borghesi, A. Krisman, T. Lu, J.H. Chen, Direct numerical simulation of a temporally evolving air/n-dodecane jet at low-temperature diesel-relevant conditions, Combust. Flame 195 (2018) 183–202.
[217] T. Zhang, B. Mei, W. Xu, Y. Ju, Experimental observations and numerical simulations of 2D cool, warm, and hot flames initiated by laser ignition, Proc. Combust. Inst. 39 (2) (2023) 1523–1531.
[218] Y. Wang, C. Xu, C. Chi, Z. Chen, Direct numerical simulations of turbulent premixed cool flames: Global and local flame dynamics analysis, Combust. Flame 270 (2024) 113759.
[219] E. Fan, W. Wang, T. Zhang, Numerical investigation on flame dynamic and regime transitions during shock–cool flame interaction, Combust. Flame 273 (2025) 113928.
[220] J. Lee, R. Knystautas, N. Yoshikawa, Photochemical initiation of gaseous detonations, Acta Astronaut. 5 (11–12) (1978) 971–982.
[221] A. Bartenev, B. Gelfand, Spontaneous initiation of detonations, Prog. Energy Combust. Sci. 26 (1) (2000) 29–55.
[222] M. Short, J. Dold, Weak detonations, their paths and transition to strong detonation, Combust. Theory Model. 6 (2) (2002) 279–296.
[223] A. Kapila, D. Schwendeman, J. Quirk, T. Hawa, Mechanisms of detonation formation due to a temperature gradient, Combust. Theory Model. 6 (4) (2002) 553–594.
[224] G. Sharpe, M. Short, Detonation ignition from a temperature gradient for a two-step chain-branching kinetics model, J. Fluid Mech. 476 (2003) 267–292.
[225] Y. Gao, P. Dai, Z. Chen, Numerical studies on autoignition and detonation development from a hot spot in hydrogen/air mixtures, Combust. Theory Model. 24 (2020) 245–261.
[226] D. Bradley, Autoignitions and detonations in engines and ducts, Philos. Trans. R. Soc. A: Math. Phys. Eng. Sci. 370 (2012) 689–714.
[227] G.T. Kalghatgi, D. Bradley, Pre-ignition and 'super-knock' in turbo-charged spark-ignition engines, Int. J. Engine Res. 13 (4) (2012) 399–414.
[228] G. Kalghatgi, Developments in internal combustion engines and implications for combustion science and future transport fuels, Proc. Combust. Inst. 35 (1) (2015) 101–115.
[229] J. Rudloff, J.-M. Zaccardi, S. Richard, J. Anderlohr, Analysis of pre-ignition in highly charged SI engines: Emphasis on the auto-ignition mode, Proc. Combust. Inst. 34 (2) (2013) 2959–2967.
[230] P. Dai, Z. Chen, S. Chen, Y. Ju, Numerical experiments on reaction front propagation in n-heptane/air mixture with temperature gradient, Proc. Combust. Inst. 35 (3) (2015) 3045–3052.
[231] P. Dai, Z. Chen, Supersonic reaction front propagation initiated by a hot spot in n-heptane/air mixture with multistage ignition, Combust. Flame 162 (11) (2015) 4183–4193.

[232] L. Bates, D. Bradley, Deflagrative, auto-ignitive, and detonative propagation regimes in engines, Combust. Flame 175 (2017) 118–122.
[233] C. Qi, Z. Chen, Effects of temperature perturbation on direct detonation initiation, Proc. Combust. Inst. 36 (2017) 2743–2751.
[234] T. Zhang, W. Sun, Y. Ju, Multi-scale modeling of detonation formation with concentration and temperature gradients in n-heptane/air mixtures, Proc. Combust. Inst. 36 (2017) 1539–1547.
[235] P. Dai, C. Qi, Z. Chen, Effects of initial temperature on autoignition and detonation development in dimethyl ether/air mixtures with temperature gradient, Proc. Combust. Inst. 36 (3) (2017) 3643–3650.
[236] F. Reinbacher, J.D. Regele, Influence of smooth temperature variation on hotspot ignition, Combust. Theory Model. 22 (3) (2018) 516–536.
[237] P. Dai, Z. Chen, Effects of NOx addition on autoignition and detonation development in DME/air under engine-relevant conditions, Proc. Combust. Inst. 37 (4) (2019) 4813–4820.
[238] J. Pan, S. Dong, H. Wei, T. Li, G. Shu, L. Zhou, Temperature gradient induced detonation development inside and outside a hot spot for different fuels, Combust. Flame 205 (2019) 269–277.
[239] P. Dai, Z. Chen, X. Gan, Autoignition and detonation development induced by a hot spot in fuel-lean and CO_2 diluted n-heptane/air mixtures, Combust. Flame 201 (2019) 208–214.
[240] A. Sow, B.J. Lee, F.E.H. Pérez, H.G. Im, Detonation onset in a thermally stratified constant volume reactor, Proc. Combust. Inst. 37 (2019) 3529–3536.
[241] J. Su, P. Dai, Z. Chen, Detonation development from a hot spot in methane/air mixtures: Effects of kinetic models, Int. J. Engine Res. 22 (8) (2021) 2597–2606.
[242] P. Dai, Z. Chen, X. Gan, M.A. Liberman, Autoignition and detonation development from a hot spot inside a closed chamber: Effects of end wall reflection, Proc. Combust. Inst. 38 (2021) 5905–5913.
[243] H.C. Lee, P. Dai, Z. Chen, X. Gan, Detonation development in PRF/air mixtures under engine-relevant conditions, Proc. Combust. Inst. 39 (2023) 4909–4918.
[244] M.B. Luong, H.G. Im, Effects of low-temperature chemistry on direct detonation initiation by a hot spot under engine conditions, Proc. Combust. Inst. 39 (4) (2023) 4989–4999.
[245] H.C. Lee, P. Dai, X. Gan, Z. Chen, Detonation development in H_2, CH_4 and PRF-air mixtures under engine-relevant conditions: From a chemical perspective, Proc. Combust. Inst. 40 (2024) 105212.
[246] A. Robert, S. Richard, O. Colin, T. Poinsot, LES study of deflagration to detonation mechanisms in a downsized spark ignition engine, Combust. Flame 162 (7) (2015) 2788–2807.
[247] L. Zhong, C. Liu, Numerical analysis of end-gas autoignition and pressure oscillation in a downsized SI engine using large eddy simulation, Energies 12 (20) (2019) 3909.
[248] T. Zhang, W. Sun, L. Wang, Y. Ju, Effects of low-temperature chemistry and turbulent transport on knocking formation for stratified dimethyl ether/air mixtures, Combust. Flame 200 (2019) 342–353.
[249] M.B. Luong, S. Desai, F.E.H. Pérez, R. Sankaran, B. Johansson, H.G. Im, A statistical analysis of developing knock intensity in a mixture with temperature inhomogeneities, Proc. Combust. Inst. 38 (4) (2021) 5781–5789.
[250] M.B. Luong, S. Desai, F.E. Hernández Pérez, R. Sankaran, B. Johansson, H.G. Im, Effects of turbulence and temperature fluctuations on knock development in an ethanol/air mixture, Flow, Turbul. Combust. 106 (2) (2021) 575–595.
[251] M.B. Luong, H.G. Im, Prediction of the developing detonation regime in a NTC-fuel/air mixture with temperature inhomogeneities under engine conditions, Proc. Combust. Inst. 39 (4) (2023) 4979–4988.
[252] P. Clavin, Z. Chen, Explosive combustion in a closed channel revisited, J. Fluid Mech. 1031 (2026) A30.
[253] P. Clavin, H. Tofaili, A one-dimensional model for deflagration to detonation transition on the tip of elongated flames in tubes, Combust. Flame 232 (2021) 111522.
[254] P. Clavin, Finite-time singularity associated with the deflagration-to-detonation transition on the tip of an elongated flame-front in a tube, Combust. Flame 245 (2022) 112347.
[255] P. Clavin, One-dimensional mechanism of gaseous deflagration-to-detonation transition, J. Fluid Mech. 974 (2023) A46.
[256] M.-H. Wu, M. Burke, S. Son, R. Yetter, Flame acceleration and the transition to detonation of stoichiometric ethylene/oxygen in microscale tubes, Proc. Combust. Inst. 31 (2) (2007) 2429–2436.
[257] W. Han, Y. Gao, C.K. Law, Flame acceleration and deflagration-to-detonation transition in micro-and macro-channels: An integrated mechanistic study, Combust. Flame 176 (2017) 285–298.
[258] M. Liberman, M. Ivanov, A. Kiverin, M. Kuznetsov, A. Chukalovsky, T. Rakhimova, Hydrogen-oxygen flame acceleration and transition to detonation in channels with no-slip walls for a detailed chemical reaction model, Phys. Rev. E 83 (5) (2011) 056313.
[259] M.-H. Wu, W.-C. Kuo, Transition to detonation of an expanding flame ring in a sub-millimeter gap, Combust. Flame 159 (11) (2012) 3414–3422.
[260] J. Yanez, M. Kuznetsov, Experimental study and theoretical analysis of a 'strange wave', Combust. Flame 167 (2016) 494–496.
[261] Y. Ballossier, F. Virot, J. Melguizo-Gavilanes, Strange wave formation and detonation onset in narrow channels, J. Loss Prev. Process. Ind. 72 (2021) 104535.
[262] H.-W. Ssu, M.-H. Wu, Formation and characteristics of composite reaction-shock clusters in narrow channels, Proc. Combust. Inst. 38 (3) (2021) 3473–3480.
[263] X. Tang, E. Dzieminska, A.K. Hayashi, N. Tsuboi, Numerical investigation of three deflagration-to-detonation transition conditions related to the velocity of the spontaneous reaction wave, Int. J. Hydrog. Energy 46 (74) (2021) 37487–37501.
[264] V. Bykov, A. Koksharov, M. Kuznetsov, V. Zhukov, Hydrogen-oxygen flame acceleration in narrow open ended channels, Combust. Flame 238 (2022) 111913.
[265] M. Vorenkamp, S.A. Steinmetz, T.Y. Chen, X. Mao, A. Starikovskiy, C. Kliewer, Y. Ju, Plasma-assisted deflagration to detonation transition in a microchannel with fast-frame imaging and hybrid fs/ps coherent anti-Stokes Raman scattering measurements, Proc. Combust. Inst. 39 (4) (2023) 5561–5569.
[266] Y. Ballossier, F. Virot, J. Melguizo-Gavilanes, Flame acceleration and detonation onset in narrow channels: Simultaneous schlieren visualization, Combust. Flame 254 (2023) 112833.
[267] P. Krivosheyev, A. Novitski, O. Penyazkov, Flame front dynamics, shape and structure on acceleration and deflagration-to-detonation transition, Acta Astronaut. 204 (2023) 692–704.
[268] P.N. Krivosheyev, V.V. Kuzmitski, O.G. Penyazkov, Experimental study of flame acceleration processes and deflagration-to-detonation transition: Review of works of the A.V. Luikov Heat and Mass Transfer Institute of the National Academy of Sciences of Belarus, Combust. Explos. Shock. Waves 59 (4) (2023) 393–401.
[269] N. Dexter-Brown, J. Jayachandran, Delineating the effects of ignition propensity and Markstein number on deflagration-to-detonation transition, Combust. Flame 265 (2024) 113439.
[270] Q. Li, H. Hu, Z. Pan, G. Ciccarelli, Transition from a fast-flame to detonation in a rough-walled channel, Combust. Flame 283 (2026) 114604.
[271] T.A. Alzer, J. Melguizo-Gavilanes, I. Wlokas, A.M. Kempf, Towards predicting deflagration-to-detonation transition in smooth channels, Proc. Combust. Inst. 42 (2026) 106093.
[272] C.C. Mejia-Botero, Flame and shock morphologies and dynamics during acceleration and transition to detonation in unobstructed channels: Effect of fundamental combustion properties (Ph.D. thesis), ISAE-ENSMA, École Nationale Supérieure de Mécanique et d'Aérotechnique - Poitiers, 2024.
[273] C.C. Mejia-Botero, F. Virot, L.F.F. da Silva, J. Melguizo-Gavilanes, Flame morphology boundaries and fundamental combustion properties in unobstructed channels, Combust. Flame 286 (2026) 114806.
[274] B. Deshaies, G. Joulin, Flame-speed sensitivity to temperature changes and the deflagration-to-detonation transition, Combust. Flame 77 (2) (1989) 202–212.
[275] L. Kagan, G. Sivashinsky, Transition to detonation of an expanding spherical flame, Combust. Flame 175 (2017) 307–311.
[276] L. Kagan, G. Sivashinsky, Parametric transition from deflagration to detonation: Runaway of fast flames, Proc. Combust. Inst. 36 (2) (2017) 2709–2715.
[277] P.V. Gordon, L. Kagan, G. Sivashinsky, Parametric transition from deflagration to detonation revisited: Planar geometry, Combust. Flame 211 (2020) 465–476.
[278] P.V. Gordon, L. Kagan, G. Sivashinsky, Parametric transition from deflagration to detonation revisited: Spherical geometry, Combust. Flame 219 (2020) 405–415.
[279] L. Kagan, P.V. Gordon, G. Sivashinsky, A reduced model for a self-accelerating expanding flame subjected to the Darrieus-Landau and Rayleigh-Taylor instabilities: Transition to detonation, Combust. Flame 246 (2022) 112420.
[280] J.A. Gray, D.A. Lacoste, Effect of the plasma location on the deflagration-to-detonation transition of a hydrogen–air flame enhanced by nanosecond repetitively pulsed discharges, Proc. Combust. Inst. 38 (4) (2021) 3463–3472.
[281] Z. Shi, X. Mao, A. Thawko, Y. Ju, Numerical modeling of plasma assisted deflagration to detonation transition in a microscale channel, Proc. Combust. Inst. 40 (2024) 105659.
[282] A. Starikovskiy, N. Aleksandrov, A. Rakitin, Plasma-assisted ignition and deflagration-to-detonation transition, Philos. Trans. R. Soc. A: Math. Phys. Eng. Sci. 370 (2012) 740–773.
[283] Y. Ju, A. Starikovskiy, Plasma Assisted Combustion and Chemical Processing, first ed., CRC Press, Boca Raton, FL, 2025.
[284] C.O. Laux, J.-B. Perrin-Terrin, V. Lafaurie, S.M. Starikovskaia, Foundations of plasma-assisted combustion: II. Mechanisms and applications, Plasma Sources Sci. Technol. 35 (2) (2026) 023002.
[285] W. Sun, X. Gao, B. Wu, T. Ombrello, The effect of ozone addition on combustion: Kinetics and dynamics, Prog. Energy Combust. Sci. 73 (2019) 1–25.
[286] X. Shi, J. Crane, H. Wang, Detonation and its limit in small tubes with ozone sensitization, Proc. Combust. Inst. 38 (3) (2021) 3547–3554.
[287] J. Sun, Z. Chen, Bifurcation of cellular detonation structure in a mixture with two-stage reactions, J. Fluid Mech. 1022 (2025) A14.
[288] W. Han, W. Liang, C. Wang, J. Wen, C.K. Law, Spontaneous initiation and development of hydrogen-oxygen detonation with ozone sensitization, Proc. Combust. Inst. 38 (2021) 3575–3583.

[289] H. Li, W. Liang, C.K. Law, Facilitated ignition and detonation initiation of hydrogen-oxygen mixtures by ozone doping, Combust. Flame 246 (2022) 112474.
[290] J. Sun, B. Tian, Z. Chen, Effect of ozone addition and ozonolysis reaction on the detonation properties of c_2h_4/o_2/Ar mixtures, Proc. Combust. Inst. 39 (3) (2023) 2797–2806.
[291] W. Han, Q. Zhang, J. Huang, Role of temperature-gradient steepness on development of hydrogen-oxygen detonation with ozone sensitization, Combust. Flame 248 (2023) 112546.
[292] H. Li, W. Liang, C.K. Law, Effects of ozone addition on direct detonation initiation in hydrogen/oxygen mixtures, Combust. Flame 257 (2023) 113052.
[293] A. Thawko, Y. Cao, Z. Shi, M. Vorenkamp, Z. Wang, B. Mei, X. Mao, Y. Ju, Accelerated ignition-shock coupling and deflagration to detonation transition by ozone kinetic enhancement of dimethyl ether mixture, Proc. Combust. Inst. 40 (2024) 105517.
[294] M. Romano, M. Radulescu, A. Higgins, J. Lee, W. Pitz, C. Westbrook, Sensitization of hydrocarbon-oxygen mixtures to detonation via cool-flame oxidation, Proc. Combust. Inst. 29 (2002) 2833–2838.
[295] M. Romano, M. Radulescu, A. Higgins, J. Lee, Sensitization of pentane-oxygen mixtures to DDT via cool flame oxidation, Combust. Flame 132 (3) (2003) 387–394.
[296] W. Liang, R. Mével, C.K. Law, Role of low-temperature chemistry in detonation of n-heptane/oxygen/diluent mixtures, Combust. Flame 193 (2018) 463–470.
[297] F. Veiga-López, Z. Weng, R. Mével, J. Melguizo-Gavilanes, Influence of low-temperature chemistry on steady detonations with curvature losses, Proc. Combust. Inst. 39 (3) (2023) 2925–2933.
[298] Z. Wang, Y. Qi, X. He, J. Wang, S. Shuai, C.K. Law, Analysis of pre-ignition to super-knock: Hot spot-induced deflagration to detonation, Fuel 144 (2015) 222–227.
[299] Y. Qi, Z. Wang, J. Wang, X. He, Effects of thermodynamic conditions on the end gas combustion mode associated with engine knock, Combust. Flame 162 (11) (2015) 4119–4128.
[300] W. Liu, Y. Qi, R. Zhang, Z. Wang, Flame propagation and auto-ignition behavior of iso-octane across the negative temperature coefficient (NTC) region on a rapid compression machine, Combust. Flame 235 (2022) 111688.
[301] Z. Wang, Y. Qi, H. Liu, P. Zhang, X. He, J. Wang, Shock wave reflection induced detonation (SWRID) under high pressure and temperature condition in closed cylinder, Shock Waves 26 (2016) 687–691.
[302] L. Yang, Y. Wang, P. Dai, Z. Chen, Effect of temperature disturbance on end-gas autoignition and detonation development, Proc. Combust. Inst. 40 (2024) 105220.
[303] G. Zhao, J. Du, H. Yang, T. Tang, M. Sun, Effects of injection on flame flashback in supersonic crossflow, Aerosp. Sci. Technol. 120 (2022) 107226.
[304] D. Yu, P. Yang, L. Yue, Z. Chen, Theoretical analysis on detonation initiation induced by thermal nonuniformity in supersonic reactive flows, Phys. Rev. Fluids 9 (2024) 103201.
[305] P. Yang, D. Yu, Z. Chen, H. Teng, H.D. Ng, Effects of thermal stratification on detonation development in hypersonic reactive flows, Phys. Rev. Fluids 9 (2024) 083202.